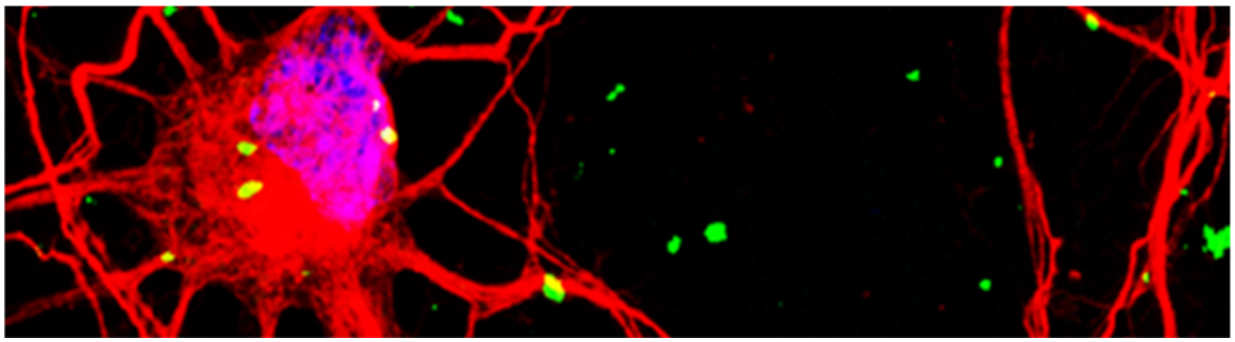

Corso di Dottorato in Neuroscienze
Curriculum Neuroscienze e Neurotecnologie
Ciclo XXXII

The role of DEPDC5 in the pathogenesis of mTOR-dependent epilepsy and focal cortical dysplasia

Candidate:
Antonio De Fusco

Supervisor:
Prof. Fabio Benfenati

ISTITUTO ITALIANO DI TECNOLOGIA

UNIVERSITÀ DEGLI STUDI DI GENOVA

Contents

1. Summary

DEP-domain containing 5 (DEPDC5) is part of the GATOR1 complex that functions as key inhibitor of the mechanistic target of rapamycin complex 1 (mTORC1) in the absence of amino acids. Mutations in DEPDC5 have been identified as the most common cause of either lesional or non-lesional focal epilepsy and are associated with mTOR hyperactivity. Recently, it has been hypothesized that somatic "second-hit" mutations occur in the brain of patients with the more severe symptomatology, including focal cortical dysplasia type II, drug-resistant epilepsy and intellectual disability. However, the mechanisms underlying dysplastic and epileptic phenotype following DEPDC5 loss-of-function, especially at the cellular levels, are still largely unknown, particularly regarding the morpho-functional impact of DEPDC5 deficiency at level of synaptic connectivity and transmission. The scope of my PhD project is to investigate the pathological changes occurring with DEPDC5 loss-of-function, with particular emphasis on cellular and synaptic morphology and physiology, and to address the role of the loss of heterozygosity in DEPDC5-related pathogenesis. As the full knockout of Depdc5 is embryonically lethal in rodents, in this study I have first characterized a heterozygous knockout mouse (Depdc5$^{+/-}$), which failed to recapitulate the major phenotypic tracts of the pathology, except for a reduced PTZ-induced epileptic threshold. Therefore, to uncover the phenotype induced by Depdc5 loss-of-function, I have compared the condition of the constitutive Depdc5$^{+/-}$ haploinsufficient mouse with the more effective acute neuronal knockdown of Depdc5 by RNA interference. While heterozygous Depdc5$^{+/-}$ neurons have a very mild phenotype with morpho-functional features that are not significantly different from wild type neurons, acutely knocked down neurons exhibit a much stronger phenotype characterized by mTOR hyperactivation, increased soma size and dendritic arborization, increased

excitatory synaptic transmission and intrinsic excitability of excitatory neurons, leading to an excitation/inhibition imbalance. These results uncover a novel synaptic phenotype that is causally linked to acute Depdc5 knockdown and mTOR hyperactivity, highlighting the loss of heterozygosity as causal factor for the establishment of FCD-related neuronal phenotype, and suggesting an involvement of Depdc5 in the neurodevelopmental processes. The robust synaptic phenotype resulting from acute sh-mediated, but not constitutive, Depdc5 deficiency is reminiscent of the somatic second-hit mechanism in patients with focal cortical dysplasia and, together with the increased intrinsic excitability, can trigger the epileptogenic process.

2. Introduction

2.1. The mTOR pathway: a general overview

The history of the mammalian target of rapamycin (mTOR) began in the early 1990s, when genetic screens in yeast identified the TOR1 and TOR2 genes as the target of the anti-proliferative effects of rapamycin, a macrolide produced by *Streptomyces Hygroscopius* bacteria, on yeast (Cafferkey et al., 1993; Kunz et al., 1993; Helliwell et al., 1994). One year later, mTOR was purified in mammals and recognized as the physical target of rapamycin (Brown et al., 1994; Sabatini et al., 1994; Sabers et al., 1995). mTOR belongs to the serine/threonine kinase protein family, and is the key point of convergence of different pathways sensitive to energy and growth factors. Its activation, through the stimulation or the inhibition of numerous signaling downstream cascades, its critical for the regulation of cell growth, survival and development (Bockaert and Marin, 2015). To exert these complex functions, mTOR associates with other proteins to form two distinct complexes named mTOR complex 1 (mTORC1) and 2 (mTORC2) (**Fig. 1**), which are differentially regulated and exert different functions (Hay and Sonenberg, 2004; Laplante and Sabatini, 2012). Indeed, mTORC1 is a sensor of nutrients (glucose, amino acids, oxygen, ATP, growth factors, neurotransmitters) and regulates fundamental functions of cellular physiology, such as protein synthesis, metabolism, autophagy and lysosome biogenesis (Laplante and Sabatini, 2012). mTORC2, instead, is preferentially activated by growth factors and controls cell shape, survival and proliferation (Laplante and Sabatini, 2012). Classical activation of mTOR by growth factors is realized through the well-characterized PI3K/Akt/TSC/Rheb pathway (Avruch et al., 2006). Indeed, growth factors bind

tyrosine kinase receptors (RTKs), which directly activate Akt. In turn, Akt phosphorylates tuberous sclerosis complex 2 (TSC2) causing its dissociation from tuberous sclerosis complex 1 (TSC1) (Inoki et al., 2002). This represents a key step for mTOR activation, since undissociated TSC1/2 exerts GTPase activity (GAP) over the small G-protein Ras homology enriched in brain (Rheb) (Inoki et al., 2003). Indeed, while GTP-bound Rheb directly activates mTORC1 (Long et al., 2005), the GAP activity of TSC1/2 in response to growth factor stimulation switches off Rheb into the inactive GDP-bound state that acts as a mTORC1suppressor.

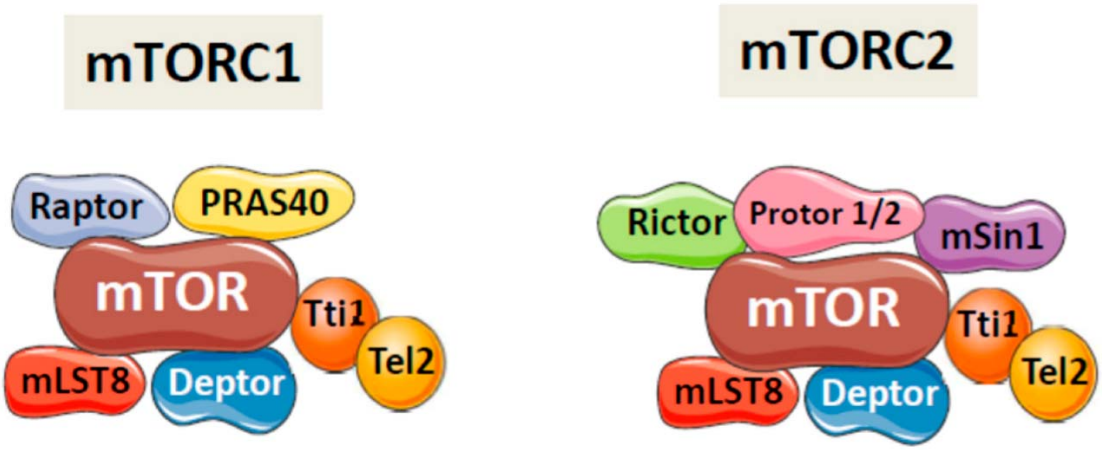

Figure 1: Components of mTORC1 and mTORC2 complexes.

mTORC1 and mTORC2 share the core proteins mTOR and mammalian lethal SEC13 protein 8 (mLST8), the Tti1/Tel2 complex and the inhibitory protein DEP domain-containing mTOR-interacting protein (DEPTOR). In addition, mTORC1 contains the regulatory-associated protein of mTOR (Raptor) and the inhibitory subunit proline-rich Akt substrate of 40 kDa (PRAS40), whereas mTORC2 contains rapamycin-insensitive companion of mTOR (Rictor) and the regulatory proteins Protor1/2 and mSin1 (from Sangüesa et al., 2019).

2.2. Effects of mTORC1 activation

The activation of mTORC1 orchestrates cellular physiological functions by integrating both intracellular and extracellular inputs. The ability to exert such functions is possible through the modulation of various effector pathways (Bockaert and Marin, 2015). Classically, translational activity is strongly enhanced by mTOR. Indeed, the control of protein synthesis is obtained through the phosphorylation of several targets, including eukaryotic translation initiation factor 4E (eIF4E)-binding proteins (4E-BP1,2,3) (Ran et al, 2013) and the p70 ribosomal S6 kinase 1 and 2 (S6K1,2) (Laplante and Sabatini, 2012). In particular, S6K1 phosphorylates the ribosomal protein S6, eukaryotic elongation factor-2 kinase (eEF2K), eIF4B, S6K1 Aly/REF (SKAR)-like substrate, a cell growth regulator, and CBP80 (cap-binding protein 80) to stimulate protein synthesis initiation (Zoncu et al., 2010). In addition, mTORC1 also promotes the biogenesis of ribosomes through the expression of ribosomal RNA (rRNA) and transfer RNA (tRNA) (Iadevaia et al., 2014). Another mechanism that contributes to the mTORC1-induced protein synthesis is the increased expression of proteasome genes, via the stimulation of the sterol regulatory element-binding protein 1 (SREBP1), that increase amino acid availability and permits better quality control of newly synthetized proteins (Zhang et al., 2014).

mTORC1 also has an important role in the lipid metabolism. Indeed, its activation promotes *de novo* lipid synthesis through the sterol-responsive element binding protein (SREBP) transcription factor, which regulates fatty acid and cholesterol biosynthesis (Porstmann et al., 2008).

mTORC1 also negatively controls macro-autophagy through the inhibition of the ULK1 complex (Unc51-like kinase 1)/Atg13 (autophagy-related genes 13)/FIP200

(focal adhesion kinase family-interacting protein) (Chen et al., 1995). In addition, the transcription of genes implicated in lysosome and autophagosome biogenesis is negatively modulated by mTORC1 (Laplante and Sabatini, 2012; Peña-Llopis et al., 2011). Energy production is also strongly affected by mTORC1 activation; indeed, it has been shown that its association with PPAR coactivator could enhance mitochondrial biogenesis and oxidative functions (Cunningham et al., 2007).

In conclusion, all the evidences stated above indicate that mTORC1 is a master regulator of a variety of cell functions, a key intracellular hub able to integrate many different extracellular inputs to orchestrate the correct cell growth, metabolism and integration with the surrounding environment.

2.3. Role of mTORC1 in neuronal physiology and pathology

mTORC1 signaling is essential for the development of an organism, since it orchestrates the growth, metabolism and correct migration of cells; indeed, it has been shown that complete loss of each one of the components of mTORC1 leads to embryonic death (Murakami et al., 2004). In addition to the functions that it exerts in every eukaryotic cell, mTORC1 signaling in the brain is also a key regulator of specific neuronal features, such as development and migration, axonal sprouting, regeneration and myelination, ion channel and receptor expression, growth of dendritic spine and synaptic plasticity (Bockaert and Marin, 2015). Most of the knowledge about the influence of mTORC1 in these processes has been obtained from studies in animal models with deletion or downregulation of its pathway.

2.3.1. Role in neuronal development and differentiation

The importance of mTOR in brain development was first observed in an ethyl-nitroso-urea-induced mouse mutation that carry a mis-spliced mutation of mTOR leading to defects in telencephalon formation and mid-gestation mortality (Hentges et al., 2001). In general, full knockout of core components of mTORC complexes results in embryonic lethality (Guertin et al., 2006; Shiota et al., 2006). Also mutations in regulatory upstream elements of mTOR have been associated with disturbances of brain development (Bockaert and Marin, 2015). It has been shown that deletion of REDD1, an upstream inhibitor of mTORC1 complex, impairs neuronal differentiation and migration (Malagelada et al., 2011). Moreover, the deletion of PTEN in the adulthood leads to constitutive neurogenesis in the subgranular zone (SGZ) of the

hippocampus and in the subventricular zone (SVZ) (Gregorian et al., 2009). In general, most of the pathologies in which the hyperactivation of mTORC1 is observed, like Tuberous Sclerosis (TS), Fragile X syndrome, Cowden syndrome, hemimegalencephaly and ganglioma are characterized by neuronal mispositioning, migratory heterotopia and cell hypertrophy (Crino et al., 2006; Ehninger, 2013; Hoeffer and Klann, 2010; Endersby and Baker, 2008; Osborne, 2010; Salamon et al., 2006).

2.3.2. Role in the somatic growth and hypertrophy

One of the most reproducible effects of enhanced mTORC1 activation in neurons is the somatic hypertrophy that has been observed in animal models after deletion of TSC1, TSC2, PTEN (Meikle et al., 2008; Zeng et al., 2008). Hypertrophy has been found in cortical neurons, hippocampal granule cells and Purkinje cells (Fraser et al., 2004; Tsai et al., 2012) and is reversed by rapamycin administration (Zeng et al., 2008), confirming that the pathogenic mechanism relies on the hyperactivation of mTORC1. Human mTORopathies also include this feature, and somatic enlargement has been consistently found in patients with TS, where the presence of giant cells within the cortical tubers is a distinctive tract of the pathology (White et al., 2001). Cytomegalic cells and "balloon" cells are also been observed in focal cortical dysplasia. The increase in soma size has been shown to impact neuronal properties. Indeed, the increase in soma size after deletion of the mTORC1 inhibitor TSC1 has been associated with decreased input resistance and increased capacitance (Bateup et al., 2011). Similar results have been found after knockdown of PTEN with small hairpin RNA (shRNA) (Luikart et al. 2011). Somatic hypertrophy also impacts neuronal functions at macroscopic level. Indeed, in animal models of TSC or PTEN deletion, the cellular

hypertrophy (potentially associated with increased neurogenesis) leads to progressive macrocephaly with increased brain size and loss of organization of cortical layers (for review see Lasarge and Danzer, 2014).

2.3.3. Role in dendritic growth and arborization

The activation of mTORC1 plays a key role also in regulating dendritic growth. It has been shown that knockdown of the mTORC1 inhibitory gene PTEN induces arborization of hippocampal neurons (Jaworski et al., 2005). While the soma and dendrite size are regulated by PI3K–Akt–mTOR pathway (Jaworski et al., 2005), its coordinated activation with the Ras-mitogen-activated protein kinase pathway also increases dendritic complexity (Kumar et al., 2005). All these effects are abolished by knockdown of mTOR and rapamycin treatment. In addition, rapamycin has been shown to inhibit BDNF-induced mTORC1 activation and dendritic growth (Jaworski et al., 2005). So, it is clear that dysregulation of the mTORC1 pathway could alter the precise development of the dendritic tree structure. This structure, however, is critical for the correct signal processing in neurons, and changes associated with mTOR disruption could alter the integration of synaptic inputs. More and thicker dendrites could mean increased connectivity among neurons and increased signal spread that could potentially be associated with abnormal network activity (Lasarge and Danzer, 2014).

2.3.4. Role in synaptic physiology and plasticity

Most of the knowledge on the effects of mTORC1 activation on synaptic activity has been obtained from studies in animal models with loss-of-function mutations and rescue with mTORC1 inhibitors and from surgical samples from TS and FCD patients. At the synaptic level, mTORC1 activation increases synaptic activity by enhancing AMPA receptor subunits GluA1 and GluA2 synthesis and surface localization (Ran et al., 2013; Wang et al., 2006). In addition, it also mediates the inhibition of Kv1.1 synthesis induced by NMDA receptor activation (Raab-Graham et al., 2006). The Sabatini's group employed a "*sparse deletion*" approach to delete TSC1 from the brain of $TSC1^{flox/flox}$ mice using a Cre-expressing virus. They found that, *in-vitro,* TSC1 KO hippocampal neurons exhibit an increased length and width of synaptic spines coupled to an increased mEPSC amplitude, without changes in frequency (Tavazoie et al., 2005). Strikingly, the same approach applied *in-vivo* yielded quite different results (Bateup et al., 2011). In this study, pyramidal neurons showed no changes in spine morphology or mEPSC amplitude, while mEPSCs frequency was increased. Successively, they demonstrated that pharmacologically blocking activity in TSC1 KO neuron cultures prevented most of the gene expression changes in these cells, suggesting that they are secondary to mTORC1 hyperactivation (Bateup et al., 2013b). TSC1 KO cells in these animals also exhibited decreased frequency and amplitude of miniature inhibitory post-synaptic currents (mIPSCs) and reduced amplitude of evoked IPSCs. These effects were reversed by rapamycin treatment, confirming that they are mTOR-dependent (Bateup et al., 2013a).

Electrophysiological recordings of human neurons from surgical samples of pediatric TS and FCD patients also revealed important properties of the abnormal neuronal types

that are present in these pathologies. Interestingly, it has been shown that giant/balloon and neuronal-glial cells from TS and FCD are unable to generate action potentials (Cepeda et al., 2005; Cepeda et al., 2003), suggesting that their role in epileptogenesis is probably negligible (Boonyapisit et al., 2003). Instead, dysmorphic/cytomegalic pyramidal neurons, both could more likely sustain the epileptiform activity in TS and FCD due to their hyperexcitability (Cepeda et al., 2005). Moreover, dysmorphic/cytomegalic pyramidal neurons have abnormal passive membrane properties, such as larger cell capacitance, longer time constant, and lower input resistance compared with normal pyramidal neurons. The amplitude of macroscopic Ca^{2+} currents and Ca^{2+} influx were also larger in this type of neurons, possibly contributing to hyperexcitability (Cepeda et al., 2003; Cepeda et al., 2012). The pathogenic role of these dysmorphic cells is also underlined by studies demonstrating cell-specific alterations in glutamate and GABA receptor subunit expression in human brain tissue from TS patients (Crino et al., 2001; Talos et al., 2008; White et al., 2001). An important role for mTORC1 has been established also in the regulation of synaptic plasticity. Indeed, the late stage of long-term plasticity (L-LTP) that requires transcription and new protein synthesis, is an mTORC1 and c-AMP dependent process (Cammalleri et al., 2003; Tang et al., 2002). Indeed, the c-AMP synthesis triggered by Ca^{2+} entry can activate mTORC1 in two different ways: (i) directly, following activation of Ca^{2+}-dependent adenylyl cyclase (Kim et al., 2010); (ii) indirectly, through the cAMP-induced release of BDNF which, in turn, activates the PI3K-Akt-mTOR pathway (Patterson et al., 2001). In contrast, other studies have shown that rapamycin application does not block L-LTP in vivo (Panja et al., 2009). The lack of S6K1 or S6K2, also, does not block normal L-LTP in mice (Antion et al., 2008). Despite the different experimental paradigms used for LTP induction could account for

these contradictory results, the exact role of mTORC1 in synaptic plasticity remains to be fully elucidated.

2.4. Role of DEPDC5 in the regulation of mTORC1

Classically, the small GTPase Rheb is considered the main regulator of mTORC1 activity (Inoki et al., 2003). Rheb is located at the lysosomal surface (Dibble et al., 2012) and is negatively modulated by the TSC complex that switch Rheb from the active GTP bound state to the inactive GDP bound state (Inoki et a., 2003). Numerous intracellular and extracellular inputs, like growth factors and energy levels regulate mTORC1 activity through this pathway (Bar-peled and Sabatini, 2014). In addition to these inputs, amino acid availability is crucial for mTORC1 activation (**Fig. 2**).

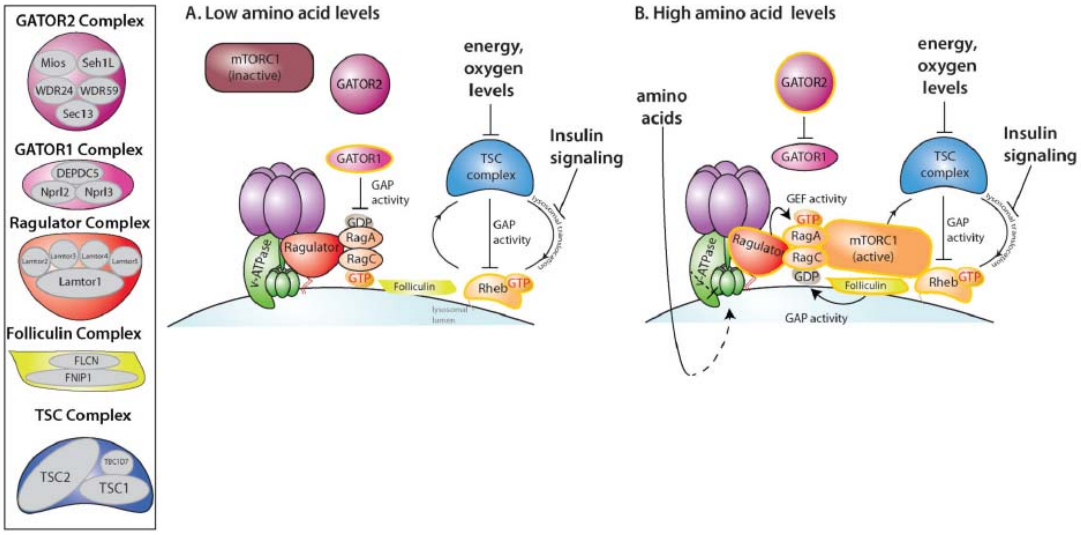

Figure 2: Schematic representation of the amino acid sensing branching of the mTOR pathway.

The GATOR2 complex, containing the proteins MIOS, SEH1L, WDR24, WDR59, and SEC13, inhibits the GATOR1 complex when there is amino acid abundance. The GATOR1 complex, containing the proteins DEPDC5, NPRL2, and NPRL3, under conditions of amino acid depletion, inhibits mTORC1 through its GAP activity towards the GTPases RagA/C (from Bar-Peled and Sabatini, 2014).

In particular, the four members of Rag proteins (Rag A, B, C, and D), expressed on the lysosomal membrane (Sekiguchi et al., 2001), are the key regulators of mTORC1 in

response to amino acids. Unlike Rheb, Rags do not directly activate mTORC1, but rather control its subcellular localization on lysosomal or late endosomal surface (Sancak et al., 2008). While under conditions of amino acid deprivation mTORC1 is diffusely distributed throughout the whole cytoplasm, when amino acids are available, it accumulates on the surface of these organelles where can be activated by Rheb (Sancak et al., 2010; Zoncu et al., 2011). Rags activity is fine regulated by a multiproteic complex, called GATOR (Bar-Peled et al., 2013) composed of two distinct interacting subcomplexes known as GATOR1 and GATOR2 that have opposite role in Rags activation. In particular, GATOR1 possesses GAP activity towards RagA, leading to its inactivation with lack of recruitment of mTORC1 at the lysosomal surface (Bar-Peled et a., 2013; Panchaud et al., 2013). GATOR1 is composed of three proteins, namely DEPDC5 (DEP domain-containing protein5), NPRL2 (nitrogen permease regulator 2-like protein) and NPRL3 (nitrogen permease regulator 3-like protein). Their specific function inside the GATOR1 complex has not been addressed, but loss-of-function of each of them has been associated with loss of amino acid regulation of mTORC1 activation (Baldassari et al., 2016). A very recent study showed that DEPDC5 phosphorylation by Pim and AKT blocks GATOR1 inhibition of mTORC1, revealing the presence of a phosphorylation-dependent regulation of DEPDC5 activity in which Pim1 and AKT act as upstream effectors of mTORC1 (Padi et a., 2019).

2.5. *DEPDC5* mutations and diseases

The *DEPDC5* gene is located on chromosome 22q12. It encodes for a protein of 1603 amino acids that is expressed ubiquitously and constantly throughout development and adulthood. Two functional domains, DUF3608 and DEP, have been identified in DEPDC5 (Dibbens et al., 2013). The DUF3608 domain accounts for the interaction of DEPDC5 with the other components of the GATOR1 complex in *yeast* (Wu and Wu, 2011), while the DEP domain is a globular domain found in other GTPase activating proteins. Loss-of-function mutation in GATOR1 components, particularly in *DEPDC5*, has been found to be the principal cause of several monogenic inherited focal epilepsies (Dibbens et al., 2013; Ishida et al., 2013; Baldassari et al., 2016; Martin et al., 2014). In affected patients, brain magnetic resonance imaging has disclosed a spectrum of Malformations of Cortical Development (MCD), ranging from Focal Cortical Dysplasia (FCD) type II to subtle band heterotopias (Scheffer et al., 2014; Baulac et al., 2015; D'Gama et al., 2017; Baldassari et al., 2019a; Baldassari et al., 2019b; Wong, 2013; Picard et al., 2014).

2.5.1. Familial focal epilepsy

Familiar Focal Epilepsies (FFEs) encompass several inherited epileptic syndromes, including autosomal dominant nocturnal frontal lobe epilepsy (ADNFLE), autosomal dominant epilepsy with auditory features (ADEAF) and familial focal epilepsy with variable foci (FFEVF). *DEPDC5* mutations are estimated to account for about 20% (range: 5-37%) of individual cases of these syndromes (Baldassari et al., 2016).

ADNFLE is a syndrome characterized by motor seizures occurring in clusters and predominantly during sleep and has been related to mutations in CHRNA4, CHRNB2 and CHRNA2. KCNT1 has been found mutated in cases with severe phenotype (Heron et al., 2012). Mutations in these genes encoding, respectively, the α4, α2 and β2 subunits of the neuronal nicotinic acetylcholine receptor (nAChRs) and a potassium channel subunit (KCNT1) account for only 10% of the pedigrees reported, suggesting further genetic heterogeneity.

ADEAF is characterized by focal seizures with typical auras and/or auditory symptoms suggesting a lateral temporal onset. Mutations in LGI1 are responsible for less than 50% of ADEAF families (Ottman et al., 2004). Efforts to identify new genes responsible for ADEAF have been unsuccessful, also because the small size of LGI1-negative pedigrees makes them not suitable for linkage analysis.

FFEVF is an autosomal dominant form of epilepsy characterized by a marked intra-familial variation. The seizures may arise from various cortical regions in different family members. Frontal and temporal (mesial and lateral) foci predominate. Nocturnal frontal phenotype is the commonest pattern described, and this may lead to misdiagnosis. Despite intra-familial heterogeneity, the individual phenotype is stereotyped (Berkovic et al., 2004).

2.5.2. Focal Cortical Dysplasia

Focal cortical dysplasia (FCD) is a clinical entity, strongly associated with intractable epilepsy (Tassi et al., 2002; Aronica and Crino, 2014) that encompasses various subtypes of cortical malformations. All subtypes are characterized by the focal

disruption of the normal cytological architecture of the cerebral cortex. The presence of dysplastic areas in the cortex is common in surgical samples from patients with epileptic focal syndromes, including autosomal dominant temporal lobe epilepsy and FFEVF. FCDs have been classified in type I, type II and type III, on the basis of differences in the neuroanatomical changes and genetic origin (Blümcke et al., 2011). In addition, different subtypes are thought to affect neurodevelopment at different stages of neurogenesis (Crino, 2015). The major hallmark of FCD type I is the abnormal cortical layering, characterized by radial microcolumns. However, this phenotype is subtle and the detection on routine neuropathology could be challenging. It can be further divided into three subtypes. FCD type Ia, in which the radial microcolumns organization resembles the early stage of cortical development; FCD type Ib, characterized by tangential layer alteration; and finally, FCD type Ic showing a combination of the other two subtypes. In all these variants, alterations in dendrite development, as well as heterotopic neurons in the white matter, could be present. FCD type IIa, in addition to the layer dyslamination observed in FCD type I, is characterized by the presence of dysmorphic/cytomegalic neuron. In addition, the presence of balloon cells defines the FCD type IIb. These cells are histologically characterized by an opalescent, eosinophilic cytoplasm and enlarged soma. FCD type II (**Fig. 3**) is a very common finding in surgical series and often causes drug-resistant focal epilepsy. Balloon cells express proteins markers of neuroglial progenitors, like SOX2, nestin and vimentin, suggesting that they originate from failures in differentiation during neurodevelopment (Orlova et al., 2010). Balloon cells are also histologically similar to giant cells found in tubers of patients with TS (Crino et al., 2006). FCD type III can include any of the alterations in cortical architecture or cell morphology present in the other subtypes, but it is also associated with brain lesions, such as tumors or vascular malformations.

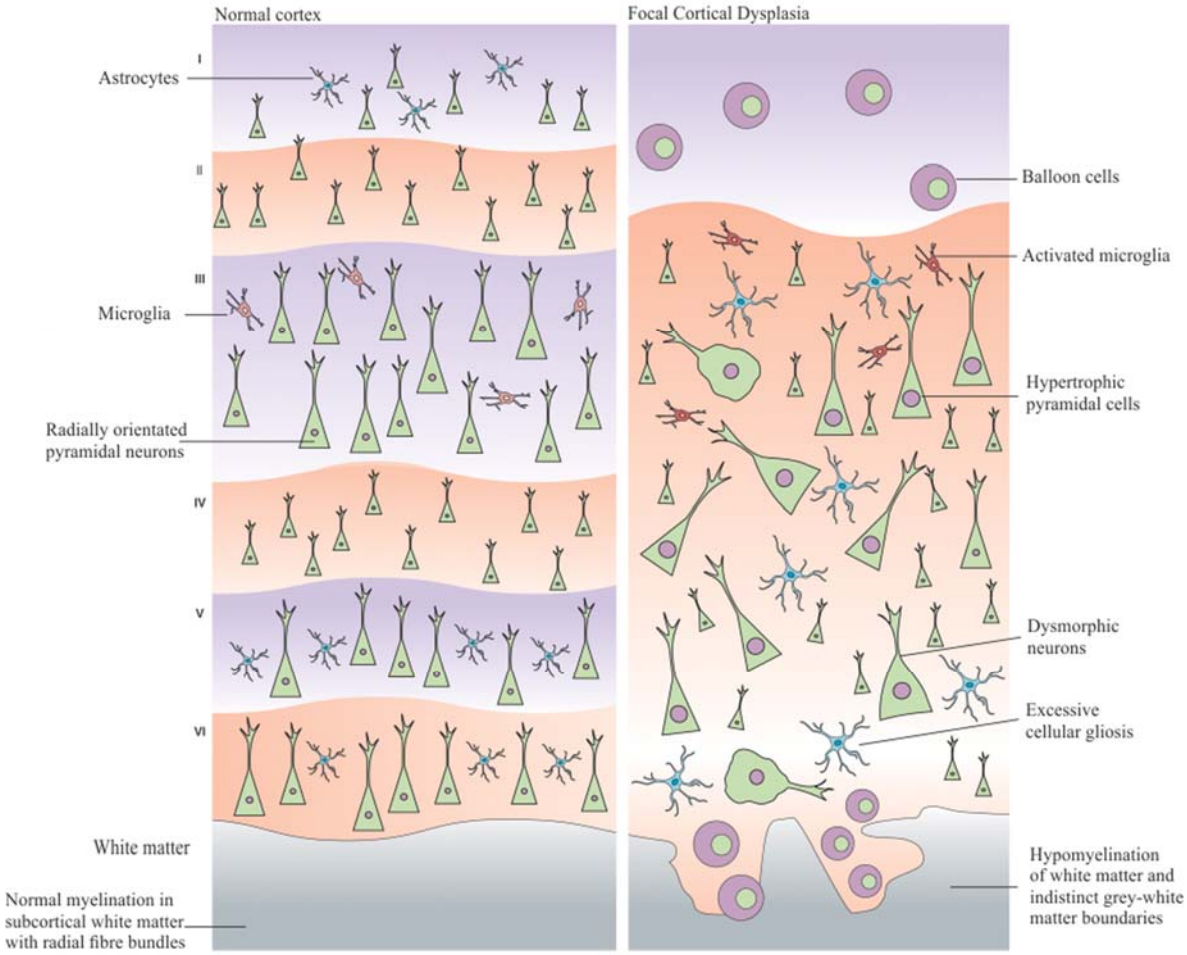

Figure 3: Schematic representation of the main histological abnormalities observed in FCD type II compared with normal brain tissue.

FCD type II, in addition to the layer dyslamination observed in FCD type I, is characterized by the presence of dysmorphic/cytomegalic neurons and balloon cells. These abnormal principal neurons are diffuse through all cortical layers (adapted from Sisodiya et al., 2009).

There are four distinct subtypes of FCD type III: the type IIIa associated with hippocampal sclerosis; IIIb, associated with tumors; IIIc, associated with vascular malformations; and IIId, associated with any other lesion.

2.6. Germline and somatic mutations of *DEPDC5*

Since the large majority of the mutations on *DEPDC5* and other GATOR1 genes leads to haploinsufficiency, the pathogenic mechanisms underlying GATOR1-related diseases has been related to loss-of-functions of these genes (Marsan and Baulac, 2018), followed by a subsequent hyperactivation of mTORC1 (**Fig. 4**).

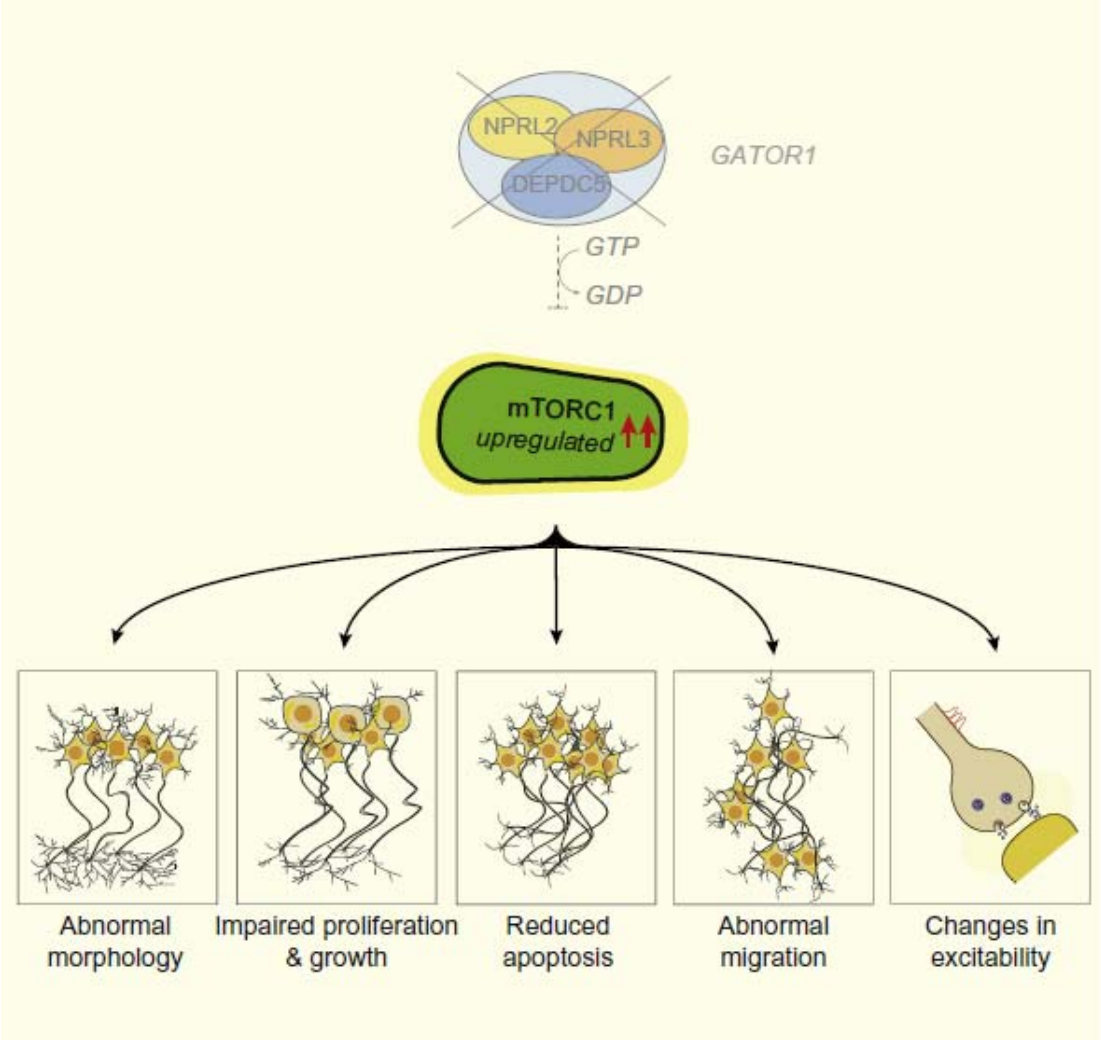

Figure 4: Effects of the abnormal activation of mTORC1.

The loss of the inhibitory brake exerted by GATOR1 upon mTORC1 upregulates the mTORC1 complex, leading to changes in morphology, proliferation, migration and apoptosis, and changes in neuronal excitability (from Baulac, 2016).

Nevertheless, the peculiar features of DEPDC5-dependent epilepsies give rise to unsolved questions. Firstly, FCD is characterized by mosaic and focal patterns, an unlikely phenotype for germline mutations. In addition, only a subset of patients carries morphological focal malformations, while the others show only non-lesional epilepsy. In resected post-operatory brain tissue, an increased phosphorylation of S6 protein has been observed only in balloon cells and dysmorphic neurons, while the large majority of cells displaying normal morphological features did not shown increased activation of the mTORC1 pathway (Marsan and Baulac, 2018). These findings seem to result from a mosaic inactivation of DEPDC5, suggesting that a double-hit inactivation in brain cells is necessary to trigger dysplastic areas. This hypothesis is based on the concept that, in individuals with a heterozygous loss-of-function mutation, a second biallelic somatic mutation on DEPDC5 occurs during neurodevelopment in a subset of progenitor cells, giving rise to the morphological abnormal cells observed in FCD. This mechanism, originally observed in cancer, is known as Knudson's two-hit mutation. Several studies on resected brain samples suggest the presence of biallelic inactivation of *DEPDC5* in patients with family history of focal epilepsy (Baulac et al., 2015; Ribierre et al., 2018; Baldassari et al., 2019b; Sim et al., 2019; Lee et al., 2019) . More recently, a study highlighted that in an individual with drug-resistant epilepsy, FCD, and a germline *DEPDC5* pathogenic variant, a second-hit *DEPDC5* variant was present and limited to dysmorphic neurons, and the somatic mutation load correlated with both dysmorphic neuron density and the epileptogenic focus (Sim et al., 2019).

2.7. Experimental models of Depdc5 loss-of-function

Given the importance of DEPDC5 mutations in the etiology of focal epilepsies and FCD, several cellular and animal models mimicking DEPDC5 haploinsuffiency have been generated. In a TALEN-mediated Depdc5 knockout rat, Marsan et al. (2016), showed that, while the constitutive deletion of Depdc5 is embryonically lethal, the heterozygous only exhibited dysmorphic pyramidal neurons and altered cortical excitability, failing to recapitulate the major tract of the pathology, i.e. the presence of spontaneous seizures (Marsan et al., 2016). These results were confirmed in a heterozygous mouse model, which also showed no increased propensity to epileptic seizures triggered by a single dose of pentylenetetrazol (Hughes et al., 2017). Interestingly, a neuron-specific Depdc5 knockout mouse was characterized by a progressive neuronal phenotype with macrocephaly, dysmorphic neurons and increased susceptibility to spontaneous and provoked seizures, up to terminal seizures (Yuskaitis et al., 2018). A morpholino oligonucleotide-mediated Depdc5 knockdown in the zebrafish was also characterized by motor hyperactivity and increased neuronal activity (de Calbiac et al., 2018), while a zebrafish full knockout model showed spontaneous epileptiform events, increased seizure propensity and premature death associated with defects in GABAergic networks (Swaminathan et al., 2018). At the cellular level, shRNA-mediated Depdc5 knockdown in mouse neuroblastoma cells or neural progenitors derived from the subventricular zone induced mTOR hyperactivation causing soma enlargement, increased filopodia formation and mislocalization of mTOR at lysosomes in the absence of amino acids (Iffland et al., 2018).

Recently, through a combination of in utero electroporation and CRISPR/Cas9 technology, it has been possible to obtain focal somatic Depdc5 deletions in the

embryonic brain. These model succeeded to reproduce the main clinical features of DEPDC5-related FCD and intractable epilepsy, displaying both dysmorphic and ectopic pyramidal neurons, cortical abnormalities, spontaneous seizures and premature sudden death due to terminal seizures (Ribierre et al., 2018; Hu et al., 2018). These studies represent the first *in-vivo* experimental evidence supporting the two-hit hypothesis as the etiology of DEPDC5-related FCD. However, the mechanisms underlying the dysplastic and epileptic phenotype following DEPDC5 loss-of-function at the cellular level are still largely unknown, particularly regarding the morpho-functional impact of DEPDC5 deficiency on synaptic connectivity, transmission and plasticity.

3. Aim of the thesis

The aim of the project is to investigate the pathological changes occurring with Depdc5 loss-of-function, with particular emphasis on cellular and synaptic morphology and functionality, and to address the role of the loss of heterozygosity in Depdc5-related pathogenesis. To address this issue, I have characterized a heterozygous Depdc5 mouse model and investigated the biochemical, morphological, ultrastructural and electrophysiological phenotypes associated with Depdc5 deficiency in two experimental models: primary heterozygous Depdc5 neurons as compared to primary WT neurons acutely silenced with an RNA interference strategy.

4. Material and methods

Experimental animals

Heterozygous Depdc5 KO mice were obtained from the IMPC European Consortium at the Sanger Institute (UK) in the frame of the European EMMA/Infrafrontier, and bred at the IIT SPF animal facility. The EUCOMM/KOMP targeting strategy was based on the "knockout-first" allele that contains an IRES:lacZ trapping cassette and a floxed neo cassette that were inserted into the intronic region between exons 4 and 5 of the *Depdc5* locus. The presence of an Engrailed (En2) splice acceptor disrupts gene function, resulting in a lacZ fusion for studying gene expression localization (Skarnes et al., 2011). Genotyping was performed by PCR with the following primers *Depdc5*_F: GGTTTTAGTTTTTGGATTTGTTTCA, *Depdc5*_R: GCCTTTAATCCCAGCACTTG; 5mut-R1_Term: GAACTTCGGAATAGGAACTTCG, that were used to detect the WT (+/+) (*Depdc5*_F plus *Depdc5*_R product, 227 bp) and mutant (*Depdc5*_F plus CAS_R1_Termproduct, 129 bp) *Depdc5* alleles and to genotype +/+ and heterozygous (+/-) mice. The colony was maintained on a C57BL/6N background and propagated in heterozygosity. Two females were housed with one male in standard Plexiglas cages (33 × 13 cm), with sawdust bedding and a metal top. After two weeks of mating, male mice were removed and dams were housed individually and daily checked for delivery. Mice were maintained on a 12:12 h light/dark cycle (lights on at 7 a.m.) at constant temperature (21 ± 1 °C) and relative humidity (60 ± 10 %). Animals were provided drinking water and a complete pellet diet (Mucedola, Settimo Milanese, Italy) *ad libitum*. Mouse genotypes were determined at weaning (P20-25) by RT-PCR on tail samples. Mice were weaned into cages of same sex pairs. Sample mice of both

genotypes were video recorded and inspected offline to monitor spontaneous behavioral seizures. All experiments were carried out in accordance with the guidelines established by the European Communities Council (Directive 2010/63/EU of March 4th, 2014) and were approved by the local Ethics Committee and the Italian Ministry of Health (authorization n. 1276/2015-PR).

Immunohistochemistry

Depdc5$^{+/+}$ and *Depdc5*$^{+/-}$ littermates (3-4 months of age) were deeply anesthetized with an intraperitoneal injection of urethane and transcardially perfused with ice-cold 0.1 M phosphate buffer (PB; pH 7.4) until the liver became clear, followed by 4% paraformaldehyde in 0.1 PB. After perfusion, brains were briefly dissected and post-fixed in the same fixative solution overnight at 4 °C. After several washes in 0.1 M PB, brains were then cryoprotected by immersion in 10, 20 and 30% sucrose solutions and subsequently cut in 30 μm sections with a Vibratome and stored at − 20 °C in a solution containing 30% ethylene glycol and 20% glycerol in 0.1 M PB. Sections containing frontal and somatosensory cortex were then washed in phosphate-buffered saline (PBS, pH 7.4) and processed for free-floating immunofluorescence. After blocking step in PBS containing 0.05% Triton X-100 and 10% normal goat serum (NGS), sections were incubated overnight at room temperature (RT) with the following primary antibodies: rabbit anti-vesicular GABA transporter (vGAT; 1:250, Synaptic System), guinea pig anti-vesicular glutamate transporter-1 (vGlut1; 1:250, Synaptic System), rabbit anti-phosphorylated S6$^{240-244}$ (pS6; 1:250, Synaptic System) or mouse anti-neuronal nuclear antigen (NeuN; 1:5000, Cell Signaling). Antibodies were diluted in PBS with 3% of NGS and 0.05% Triton X-100. Double immunofluorescence (pS6-NeuN or vGlut1/vGAT) was performed with the simultaneous addition of the primary antibodies. Sections were then washed in PBS (4 × 10 min) and incubated for 1 h at 25

°C with anti-rabbit Alexa Fluor 488, and anti-mouse Alexa Fluor 568 or anti-guinea pig Alexa Fluor 488 (Invitrogen). After several PBS rinses, sections were mounted on glass slide and observed with a Leica SP8 confocal microscope (Leica Microsystem). Z-series stacks of seven consecutive confocal sections (1024x1024 pixels) for a total depth of 2 µm of tissue were acquired at 20 x using the multi-track mode to avoid fluorescence crosstalk (pinhole: 1.0 airy unit) and background labeling was subtracted. Sections of frontal or somatosensory cortices were reconstructed and analyzed using ImageJ.

RNA extraction, retrotranscription and qRT-PCR

Total cellular or tissue RNA was extracted using TRIzol (Life Technologies). RNA concentration was quantified by using theNanodrop-1000 spectrophotometer (Thermo Scientific). cDNA was synthesized starting from 0.25 µg RNA with SuperScript IV Reverse Transcriptase kit (#18090010; Thermo Fisher) according to manufacturer's instruction and used for qRT-PCR. Gene expression was measured by quantitative real-time PCR using C1000 Touch™ Thermal Cycler (Bio-Rad) on a CFX96™Real-Time System following the manufacturer's protocol. Real time PCR analyses were performed using the SYBR Green I Master mix (Roche), on a Lightcycler 480 (Roche), with the following protocol: 95 °C for 5 min; 10s at 95 °C / 20 s at the specific annealing temperature (Ta) / 10 s at 72 °C for 45 cycles; melting curve (heating ramp from 55 °C to 95 °C) in order to check for amplification specificity. The following primers (final concentration 0.25 µM) and annealing temperature were used:

*Depdc5*_F: TGATGCCTACGATGCTCAAG, Ta= 64 °C;

*Depdc5*_R: TGGCTCCTCACTTCCTCAGT, Ta= 64.1 °C;

*Gapdh*_F: GATCATCAGCAATGCCTCCT, Ta= 59.8 °C;

*Gapdh*_R: TGTGGTCATGAGTCCTTCCA, Ta= 61.7 °C;

Relative gene expression was determined using the ΔΔCT method, normalizing data the housekeeping transcript (*Gapdh*).

Pentylenetetrazol-induced seizures

Depdc5$^{+/+}$ and *Depdc5*$^{+/-}$ littermates (3-4 months of age) were repeatedly injected with unitary doses of pentylenetetrazol (PTZ; 10 mg/kg intraperitoneally in 0.9% saline) every 10 min and continuously monitored after each injection in a 17x17x25 cm box equipped with the Anymaze video tracking system. Seizure scoring was conducted as previously reported by Browning and Nelson (1986), and the following parameters were considered: (i) myoclonic jerk, (ii) face and forelimb clonus (iii) whole body clonus with twisting or loss of posture, (iv) running/bouncing clonus, (v) tonus: (tonic flexion and tonic extension). At the end of the observation period, animals were killed humanely by cervical dislocation. Seizure manifestations were recorded by inspection of the videos by two independent observers blind to the genotype. Seizure threshold was defined as the dose (mg/kg) necessary to induce a score (v).

Plasmids and viral vectors

Four distinct short hairpin (sh) RNAs (Origene, TL508165) and a scramble (Scr) construct (Origene, TR30023) in a pGFP-C-Lenti vector were used to acutely silence *Depdc5* expression. Sequences were:

sh1: AAGTGAGGAGCCAGGCTTCTGATGACACG

sh2: GTGGACCAGACTGTGACTCAAGTATTCCG

sh3: TGTCCGACCTGGAGGATACACGCCTCAGA

sh4: CTCCAGTCGGCAAGAAAGGAACCTCAGCT

Lentiviral particles encoding these vectors are a modification of Addgene plasmids 8454, 8455 co-expressing turbo-Green Fluorescent Protein (tGFP) as a reporter and

were produced as previously described (Stewart et al., 2003) at the Virus Core Facility, Charité University, Berlin, Germany.

Culture and transfection of cell lines.

HEK-T293 cells were cultured in Dulbecco's MEM (DMEM; Gibco) supplemented with 10% fetal calf serum (Gibco), 1% L-glutamine, 100 U/ml penicillin, and 100 µg/ml streptomycin (Gibco) and maintained at 37 °C in a 5% CO^2 humidified atmosphere. For transfection experiments Lipofectamin2000 (Thermo Scientific) was used according to the manufacturer's protocol, and cells were incubated under standard growth conditions for 72 h and then processed.

Cultures and transduction of primary neurons

Low-density cortical neurons were prepared from WT C57BL/6J (Charles River) for RNA interference experiments or from *Depdc5*$^{+/+}$ and *Depdc5*$^{+/-}$ C57BL/6N mice, as previously described (Baldelli et al. 2007; Chiappalone et al. 2009). Animals were sacrificed by CO_2 inhalation and 17/18-day embryos (E17-18) were immediately removed by cesarean section. In brief, cerebral cortices were dissociated by enzymatic digestion in 0.125% trypsin for 20 min at 37 °C and then triturated with a fire-polished Pasteur pipette. Primary cultures of dissociated cortical neurons were subsequently plated onto poly-D-lysine (0.1 mg/ml, Sigma-Aldrich)-coated 25-mm glass coverslips ($6x10^4$ cells/coverslip) and 35-mm wells (1×10^6 cells/well). Neurons were maintained in a culture medium consisting of Neurobasal (Gibco) supplemented with B27 (1:50 v/v, Gibco), Glutamax (1% w/v, Gibco), penicillin–streptomycin (1%, Gibco) and kept at 37 °C in a 5% CO_2 humidified atmosphere. For shRNA transfection experiments, neurons ($4x10^6$) were nucleofected before with Amaxa basal nucleofector kit for primary neurons (Lonza) with 4 µg of plasmid DNA according to the manufacturer's

protocol. For lentiviral transduction experiments, 7 DIV cortical neurons were infected with lentiviruses at 10 multiplicity of infection (MOI). After 24 h, the medium was replaced with an equal volume of fresh and conditioned medium (1:1). All experiments were performed 5-6 days post-infection, when not differently indicated. Transduction efficiency was always above 75% of neuronal cells.

Western blotting

Total cell lysates were obtained from cortical neuronal cultures or whole brains from E12.4 mouse embryos. Cells were extracted in lysis buffer (150 mM NaCl, 50 mM Tris-HCl pH 7.4, 1 mM EDTA, 1% Triton X-100) supplemented with protease and phosphatase inhibitor cocktails (Roche, Monza, Italy). After 10 min of incubation on ice, cell lysates were collected and clarified by centrifugation (10 min at 10,000 x g at 4 °C). Brains were dissected and pottered in liquid nitrogen, then centrifuged at 1,000 x g for 10 min at 4 °C. Protein concentration was determined using BCA (Thermo Scientific) assay. Equivalent amounts of protein were subjected to SDS-PAGE on 10% polyacrylamide gels and blotted onto nitrocellulose membranes (Whatman). Blotted membranes were blocked for 1 h in 5% milk in Tris-buffered saline (10 mM Tris, 150 mM NaCl, pH 8.0) plus 0.1% Triton X-100 and incubated overnight at 4 °C with the following primary antibodies: rabbit anti-Depdc5 (1:1000, Abcam, ab185565), rabbit anti-phosphorylated S6 protein (1:2000, Cell Signaling, #2215), mouse anti-S6 (1:1000, Cell Signaling, #2317), mouse anti-Actin (1:2000, Sigma-Aldrich, A2228). Membranes were washed and incubated for 1 h at RT with peroxidase-conjugated goat anti-mouse (1:3000; Bio-Rad) or anti-rabbit (1:5000; Bio-Rad) antibodies. Bands were revealed with the ECL chemiluminescence detection system (Thermo Scientific) and the quantification of immunoreactivity was performed by densitometric analysis of the fluorograms.

Patch-clamp recording in primary cortical neurons.

Whole patch-clamp recording were made from primary cortical neurons as previously described (Baldelli et al. 2007; Chiappalone et al. 2009) using a Multiclamp 700B/Digidata1440A system (Molecular Devices, Sunnyvale, CA). Patch pipettes, prepared from thin borosilicate glass, were pulled and fire-polished to a final resistance of 4-5 MΩ when filled with standard internal solution. For all the experiments, cells were maintained in standard extracellular Tyrode solution containing (in mM): 140 NaCl, 2 $CaCl_2$, 1 $MgCl_2$, 4 KCl, 10 glucose, and 10 HEPES (pH 7.3 with NaOH). For the analysis of neuronal excitability, D-(−)-2-amino-5-phosphonopentanoic acid (D-AP5; 50 μM), 6-cyano-7 nitroquinoxaline-2,3-dione (CNQX; 10 μM), bicuculline methiodide (30 μM), and (2S)-3-[[(1S)-1-(3,4-dichlorophenyl)ethyl]amino-2-hydroxypropyl] (phenylmethyl)phosphinic acid hydrochloride (CGP58845; 5 μM) were added to block NMDA, non-NMDA, $GABA_A$, and $GABA_B$ receptors, respectively. Current-clamp recordings of AP firing activity were performed at a holding potential of −70 mV and APs were induced by injection of 10 pA current steps lasting 500 ms in morphologically identified pyramidal neurons. Excitatory neurons were identified by estimating the AP failure ratio evoked by short trains of high-current steps at increasing frequency (10-140 Hz; Prestigio et al., 2019). The mean firing frequency was calculated as the number of APs evoked by minimal current injection in 500 ms, whereas the instantaneous frequency was estimated as the reciprocal value of the time difference between the first two evoked APs. Current-clamp recordings of APs were acquired at a 50 kHz and filtered at 1/5 of the acquisition rate with a low-pass Bessel filter. The mean firing frequency and the instantaneous frequency were analyzed using Clampfit 10.7 (Molecular Devices, Sunnyvale, CA) and Prism softwares. The shape properties of the first AP elicited by minimal current injection were analyzed by

building time-derivatives of voltage (dV/dt) *versus* voltage plots (phase-plane plots) as previously described (Valente et al., 2016; Prestigio et al., 2019). Phase-plane plots were obtained and analyzed with the software OriginPro-8 (OriginLab Corp., Northhampton, MA, USA). For recording miniature excitatory postsynaptic currents (mEPSCs), bicuculline, CGP58845, D-AP5 and tetrodotoxin (TTX; 300 nM) were added to the extracellular solution to block $GABA_A$, $GABA_B$, NMDA receptors and generation and propagation of spontaneous action potentials (APs). For miniature Inhibitory Postsynaptic Currents (mIPSCs), D-AP5, CGP58845, CNQX and TTX (300 nM) were added in the Tyrode extracellular solution. The internal solution (K-gluconate) used for recording APs in current-clamp and mEPSCs in voltage-clamp configuration contained (in mM): 126 K gluconate, 4 NaCl, 1 $MgSO_4$, 0.02 $CaCl_2$, 0.1 BAPTA, 15 glucose, 5 Hepes, 3 ATP, and 0.1 GTP (pH 7.3 with KOH). The internal solution (KCl) used for mIPSC recordings contained (in mM): 126 KCl, 4 NaCl, 1 $MgSO_4$, 0.02 $CaCl_2$, 0.1 BAPTA, 15 glucose, 5 Hepes, 3 ATP, and 0.1 GTP (pH 7.3 with KOH). All the reagents were from Tocris, otherwise specified. Both mEPSCs and mIPSCs were acquired at a 10 kHz sample frequency and filtered at 1/5 of the acquisition rate with a low-pass Bessel filter. The amplitude and frequency of the miniature excitatory and inhibitory events were calculated using a peak detector function using appropriate threshold amplitudes and areas. The frequency, amplitude and kinetics of miniature PSCs were analyzed using the MiniAnalysis (Synaptosoft) and Prism (GraphPad Software, Inc.) software. All experiments were performed at RT.

Immunocytochemistry

Primary cortical neurons were fixed in 4% formaldehyde, freshly prepared from paraformaldehyde, in 0.1 M PB, pH 7.4 for 20 min at RT and immunostained for specific pre/postsynaptic markers of excitatory and inhibitory synapses. Briefly, after

several washes in PBS, cells were permeabilized and blocked for 30 min in 0.05% Triton X-100 and 10% normal goat serum (NGS) in PBS and then incubated overnight with primary antibodies diluted in 3% NGS and 0.05% Triton X-100 in PBS. Antibodies were used as follows: mouse anti-S6 protein (Cell Signaling, #2317), rabbit anti-phosphorylated-S6 protein (Cell Signaling, #2215), guinea pig anti-vGlut1 (1:500, Synaptic Systems, 135 304), mouse anti-Homer1 (1:200; Synaptic Systems, 160 011), rabbit anti-vGAT (1:500; Synaptic Systems 131 003), mouse anti-Gephyrin (1:500; 147 011), rabbit anti-GluA1 (1:500; Synaptic Systems, 182 003), rabbit anti-$GABA_A$-β2 receptor subunit (1:500; Synaptic Systems, 224 803). Neurons were then washed three times in PBS and then incubated in the same buffer with Alexa-conjugated secondary antibodies (1:1500, Invitrogen) and counterstained with Hoechst for nuclei detection. After several washes in PBS, coverslips were mounted with Moviol mounting medium. Images were acquired using a 40x objective with a Leica SP8 confocal microscopy (Leica Microsystems, Wetzlar, Germany). Images were processed using the colocalization plugin of ImageJ. For the analysis of synaptic density, basal dendrites of neurons were considered, and the colocalization analysis was performed, after threshold subtraction, to evaluate the simultaneous presence of pre- and a post-synaptic markers (vGlut1/Homer1 for excitatory synapses and vGAT/Gephyrin for inhibitory synapses). For experiments with transduced neurons, only tGFP-positive neurons were analyzed. To identify *bona fide* synaptic boutons, we selected colocalized puncta within an area of 0.1-1 μm^2, corresponding to the overlapping area of pre-synaptic and post-synaptic proteins. We counted the number synaptic puncta present within 30 μm dendrite tracts starting from the cell body. For the analysis of postsynaptic receptors, the thresholded signal of Homer1 and Gephyrin was overlapped to GluA1 and $GABA_A$-β2 receptors, respectively, and the fluorescence intensity was measured only within this colocalization area. Data are referred to three

independent experiments carried out in duplicate with 5-10 neurons analyzed per duplicate.

Electron Microscopy

Low-density cultures of cortical neurons from *Depdc5*$^{+/+}$ and *Depdc5*$^{+/-}$ embryos, or from WT C57BL/6J embryos infected at 7 DIV with either shScr or sh*Depdc5* lentiviruses were processed for transmission electron microscopy (TEM). Neurons were fixed at 14-15 DIV with 1.2% glutaraldehyde in 66 mM sodium cacodylate buffer, post-fixed in 1% OsO_4, 1.5% $K_4Fe(CN)_6$, 0.1 M sodium cacodylate, *en bloc* stained with 10% of uranyl acetate replacement stain (EMS) for 30 min, dehydrated, and flat embedded in epoxy resin (Epon 812, TAAB). After baking for 48 h, the glass coverslips were removed from the Epon block by thermal shock and neurons were identified by means of a stereomicroscope. Embedded neurons were excised from the block and mounted on a cured Epon block for sectioning using an EM UC6 ultramicrotome (Leica Microsystems). Ultrathin sections (60-70 nm thick) were collected on 200-mesh copper grids (EMS) and observed with a JEM-1011 electron microscope (Jeol, Tokyo, Japan) operating at 100 kV using an ORIUS SC1000 CCD camera (Gatan, Pleasanton, CA). For each experimental condition, at least 30 images of synapses were acquired at 10,000x magnification (sampled area per experimental condition: 36 μm^2). Synaptic vesicles (SVs) were defined as spherical organelles with a diameter of approximately 40 nm. Synaptic morphological features, including nerve terminal area, active zone (AZ) length, number and density of total SVs and of AZ-docked SVs were determined using ImageJ.

Statistical analysis

Data are expressed as means ± SEM or box plot showing median, mean, 25^{th} to 75^{th} interquartile range and min to max values for number of cells (N) or independent preparations as detailed in the figure legends. Normal distribution of data was assessed using the D'Agostino-Pearson's normality test ($n>6$) or the Shapiro-Wilk test ($n\leq6$). The F-test was used to compare variance between two sample groups. To compare two experimental groups, either the two-tailed unpaired Student's *t*-test or the non-parametric Mann-Whitney's *U*-test was used based on data distribution. To compare more than two normally distributed experimental groups, one-way ANOVA (followed by the Bonferroni's multiple comparison test) or repeated measures ANOVA was used. To compare more than two experimental groups that are not normally distributed, the Kruskal-Wallis ANOVA was used, followed by the Dunn's multiple comparison test. Significance level was preset to $p<0.05$. Statistical analysis was carried out using Prism (GraphPad Software, Inc., La Jolla, CA).

5. Results

5.1. Validation of Tm1a cassette efficiency

As previously assessed in other murine models of constitutive *Depdc5* knockout (Marsan et al., 2016; Hughes et al., 2017), homozygous deletion of *Depdc5* leads to prenatal mortality (occurring between E14.5 and E17.5); consistently, we have never observed *Depdc5*$^{-/-}$ newborn after mating heterozygous to heterozygous carriers. Thus, to verify the block of *Depdc5* gene expression obtained by the insertion of the Tm1a allele (**Fig. 5A**), we evaluated *Depdc5* mRNA and protein levels by means of Real-Time qPCR and Western Blotting, respectively, in the whole brain of E12.5 *Depdc5*$^{+/+}$, *Depdc5*$^{+/-}$ and *Depdc5*$^{-/-}$ embryos (**Fig. 5B,C**). The analysis confirmed that *Depdc5* mRNA levels were significantly reduced in *Depdc5*$^{+/-}$ and *Depdc5*$^{-/-}$ embryos by ≈ 40% and ≈ 90%, respectively, compared to *Depdc5*$^{+/+}$ littermates (p=0.0016, One-Way ANOVA test). However, when we performed Western Blotting analysis, we observed that Depdc5 protein levels were reduced of ≈ 50% in *Depdc5*$^{+/-}$ and 100% in *Depdc5*$^{-/-}$ embryos (**Fig. 1C**; p=0.002, Student's *t*-test). Thus, despite the qRT-PCR showed a residual *Depdc5* mRNA in *Depdc5*$^{-/-}$ embryos, the total absence of Depdc5 protein in *Depdc5*$^{-/-}$ embryos indicates that the insertion of the Tm1a allele was 100% efficient in disrupting gene expression and that the residual transcript traces did not lead to protein translation.

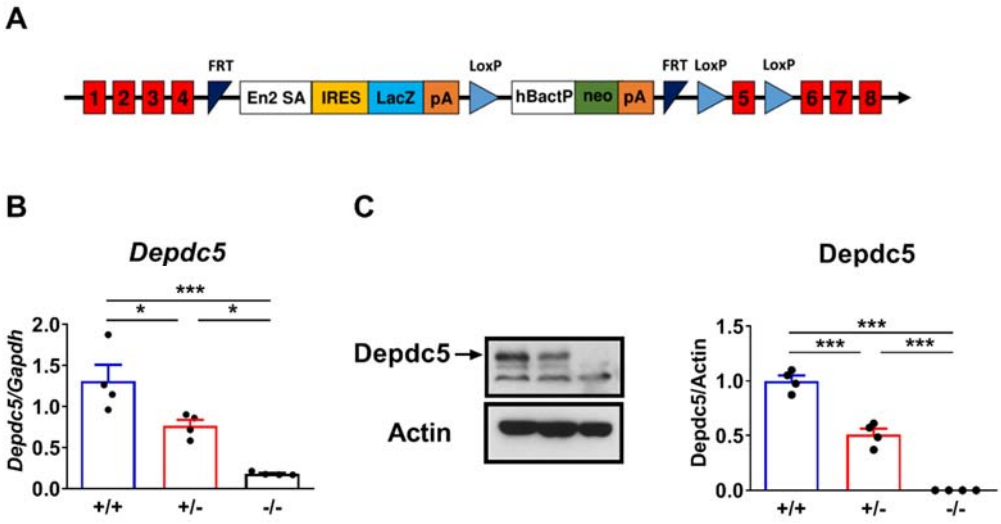

Figure 5: Characterization of constitutive Depdc5 knockdown model.

A. *Representative image showing the insertion cassette of the Tm1a allele carried by Depdc5 mouse.* ***B.*** *Bar plots showing Depdc5 mRNA levels in* $Depdc5^{+/+}$, $Depdc5^{+/-}$ *and* $Depdc5^{-/-}$ *embryos.* ***C****. Representative Western Blot images (left) and bar plot (right) showing Depdc5 protein levels in* $Depdc5^{+/+}$, $Depdc5^{+/-}$ *and* $Depdc5^{-/-}$ *embryos. Data are expressed as means ± SEM with individual experimental points. *p<0.05; ***p<0.001, Kruskal-Wallis ANOVA/Dunn's test.*

5.2. Morphological characterization of the Depdc5 heterozygous mouse

Given the importance of *DEPDC5* mutations in mTOR-dependent FCD etiology (Baulac et al., 2015; Baldassari et al., 2019a), we assessed the level of activation of mTORC1 pathway and checked for subtle alterations in cortical architecture in *Depdc5*$^{+/-}$ mice. First, we assessed the phosphorylation levels of S6 protein (a widely accepted marker for mTORC1 activation) in cortical lysates from 3-months old *Depdc5*$^{+/+}$ and *Depdc5*$^{+/-}$ mice (**Fig. 6 A,B)**, but the analysis revealed no significant changes between *Depdc5*$^{+/+}$ and *Depdc5*$^{+/-}$ mice (**Fig. 6, B**). We thus could confirm that, as already reported (Marsan et al., 2016; Hughes et al., 2017), heterozygous loss of function of *Depdc5* fails to hyperactivate mTORC1 pathways *in vivo*. Immunostaining analysis, however, revealed that heterozygous mice had a significantly increased number of pS6-positive neurons in cortical sections from frontal (p=0.0006, Mann-Whitney *U*-test) and somatosensory (p=0.005, Mann-Whitney's *U*-test) cortices (**Fig. 6C,D**). Interestingly, the increase of pS6-positive cells was specifically localized in layers IV and VI, in both frontal (**Fig. 6D**, *middle*) and somatosensory (**Fig. 6D**, *bottom*) cortices. However, when we measured the total cortical thickness, as well as single layer thickness in slices stained with the Neuronal Nuclear Marker (NeuN), no significant differences between *Depdc5*$^{+/+}$ and *Depdc5*$^{+/-}$ mice were detected (**Fig. 7**), ruling out an overt disturbance in the central nervous system development or in neuronal migration.

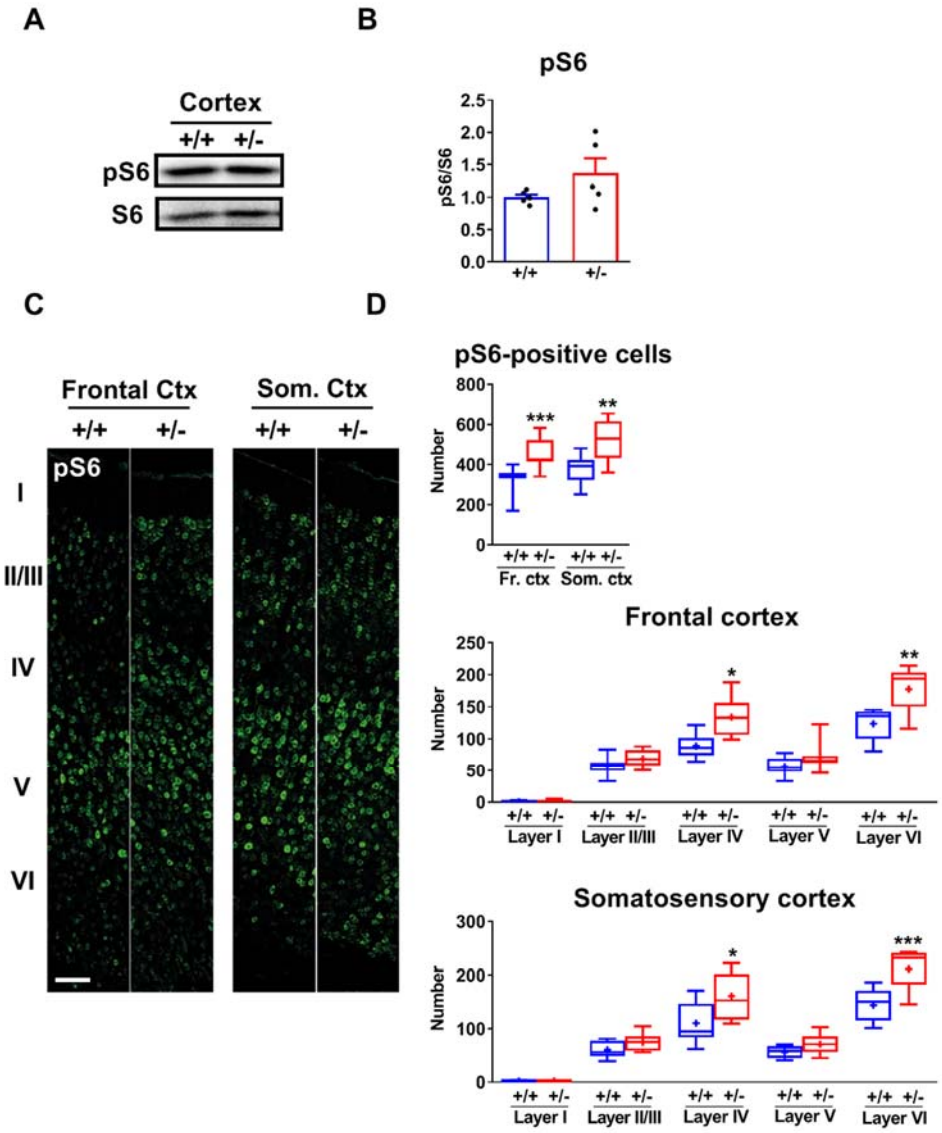

Figure 6: Depdc5$^{+/-}$ mice do not display hyperactivation of the mTORC1 pathway.

A,B. *Representative Western Blot images* ***(A)*** *and histogram* ***(B)*** *showing the phosphorylation level of S6 protein in cortices from Depdc5$^{+/+}$ and Depdc5$^{+/-}$ mice.* ***C.*** *Representative confocal cortical reconstruction of frontal (left) and somatosensory (right) cortices of Depdc5$^{+/+}$ and Depdc5$^{+/-}$ mice stained for pS6.* ***D.*** *Morphometric analysis of the number of pS6 positive cells in total cortical sections (up) and the number of pS6-positive cells in defined layers of the frontal (middle) and somatosensory cortices, respectively (bottom). Data are shown as box plots. *p<0.05; **p<0.01; ***p<0.001, Student's t-test/Mann Whitney's U-test. Scale bar: 100 μm.*

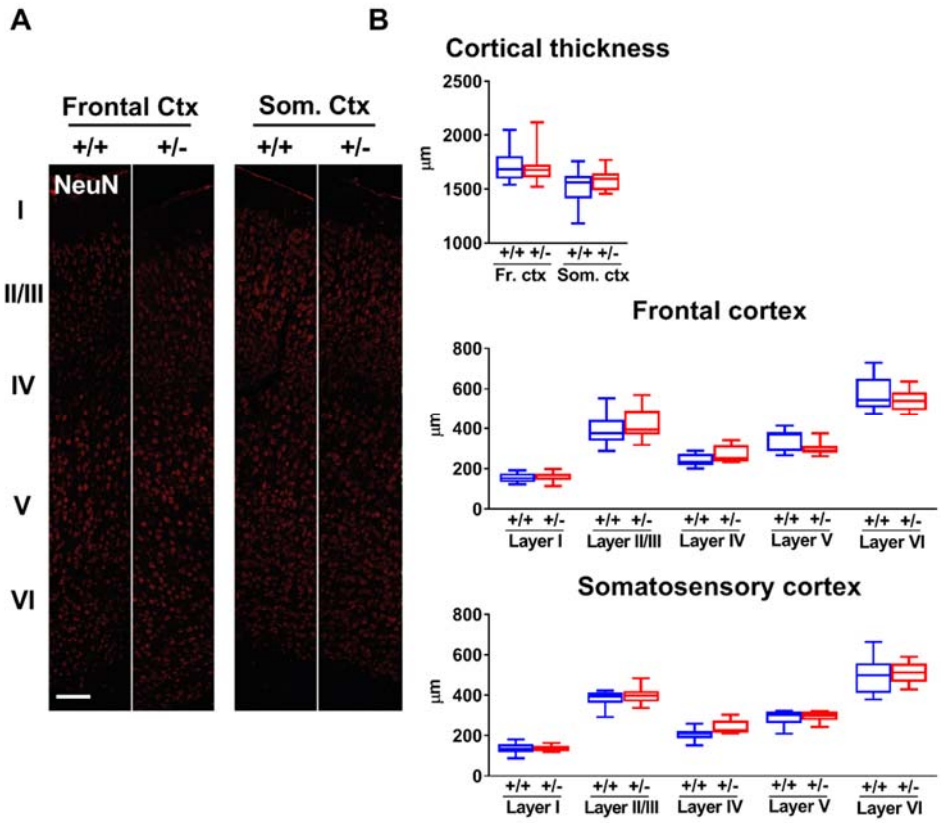

Figure 7: Cortical layer thickness is not altered in Depdc5$^{+/-}$ mice.

A. *Representative confocal cortical reconstruction of frontal (left) and somatosensory (right) cortices of Depdc5$^{+/+}$ and Depdc5$^{+/-}$ mice stained for NeuN.* ***B.*** *Morphometric evaluation of total cortical (up) and single layer thickness in the frontal (middle) and somatosensory (bottom) cortices of Depdc5$^{+/+}$ and Depdc5$^{+/-}$ mice, respectively. Data are shown as box plots. No significant differences were found (Student's t-test/Mann Whitney's U-test). Scale bar: 100 µm.*

5.3. Increased seizure susceptibility of *Depdc5*$^{+/-}$ mice

Alterations in the balance between excitation and inhibition, occurring either locally or diffused to the whole brain, are believed to be at the basis of most epileptic phenotypes (Stafstrom, 2014; Bozzi et al., 2018). We then assessed whether *Depdc5* mutants displayed any excitatory/inhibitory imbalance in synaptic connectivity by counting, in cortical sections, puncta positive for vGlut1 and vGAT, which are presynaptic markers of excitatory and inhibitory synapses, respectively (**Fig. 8A,B**), in 3-months old *Depdc5*$^{+/+}$ and *Depdc5*$^{+/-}$ mice. Interestingly, heterozygous mice showed an increased vGlut1/vGAT ratio in both frontal and somatosensory regions (p=0.042 and p=0.010, respectively, Student's *t*-test; **Fig. 8A,B**), opening the possibility that these *Depdc5* mutants display a pro-epileptic phenotype. Indeed, despite *Depdc5*$^{+/-}$ mice did not display spontaneous seizures, as assessed by long-term video-tracking, the potential excitatory/inhibitory imbalance suggests that a subtle epileptic phenotype could be present in *Depdc5*$^{+/-}$ mice. Indeed, *Depdc5*$^{+/-}$ mice challenged with the serial administration of low-doses of the convulsant pentylentetrazol (PTZ, 10 mg/kg every 10 min, until provocation of a tonic-clonic seizure) displayed a significantly lower seizure threshold than *Depdc5*$^{+/+}$ littermates (p=0.039, Student's *t*-test; **Fig. 8C**).

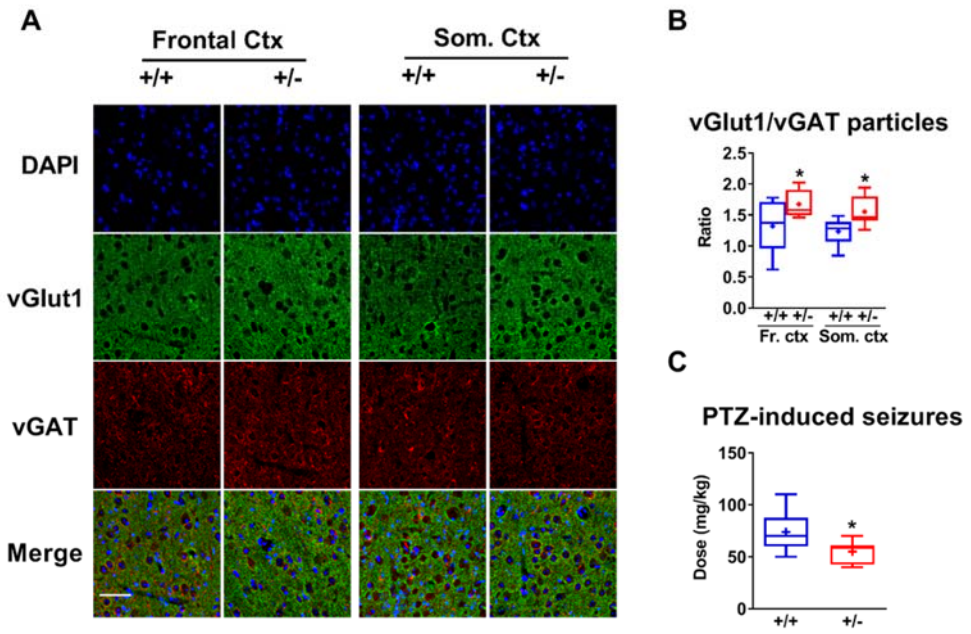

Figure 8: Depdc5$^{+/-}$ mice display lowered PTZ-induced seizure threshold.

A,B. *Representative confocal images of DAPI, vGlut1, vGAT staining, and overlapped signals in frontal (left) and somatosensory (right) cortices of Depdc5$^{+/+}$ and Depdc5$^{+/-}$ mice* ***(A)*** *and ratio between vGlut1- and vGAT-positive puncta in the frontal (left) and somatosensory (right) cortices of Depdc5$^{+/+}$ and Depdc5$^{+/-}$ mice* ***(B)****.* ***C.*** *Seizure provocation threshold in Depdc5$^{+/+}$ and Depdc5$^{+/-}$ mice (n=8/genotype) treated with progressively increasing doses of the convulsant PTZ. Data are shown as box plots. *p<0.05; Student's t-test/Mann Whitney's U-test. Scale bar: 50 µm.*

5.4. Validation of the shRNA-induced Depdc5 deficiency model

Our previous experiments showed that the *Depdc5*$^{+/-}$ mouse fails to recapitulate the major traits of DEPDC5-related pathological phenotype, namely the cytoarchitectural malformations in the cerebral cortex and the occurrence of spontaneous seizures. The presence of mosaic loss of heterozygosity has been often observed in the brain of patients with FCD and epilepsy, suggesting that heterozygous haploinsufficiency could be not sufficient to trigger the most severe effects of DEPDC5 deficiency. Thus, in the effort to induce a stronger Depdc5 depletion in neurons, reminiscent of loss of heterozygosity, we adopted a RNA interference strategy and designed four distinct anti-*Depdc5* shRNA constructs (sh1-sh4). We independently transfected the constructs in HEK-293T cells and evaluated *Depdc5* transcript levels by qRT-PCR analysis. All shRNAs significantly reduced Depdc5 mRNA levels compared to the scrambled construct with a more intense Depdc5 mRNA down-regulation by the sh3 (≈70% decrease; p=0.008, Kruskal-Wallis ANOVA/Dunn's tests; **Fig. 9A**). The sh3 construct was therefore used for subsequent experiments. We transduced cultured primary neurons with lentiviral vectors encoding for either the sh3 against *Depdc5* mRNA (*Depdc5*^{KD1}) or a scramble construct thereof (*Depdc5*^{Scr}). We found that *Depdc5*^{KD1} neurons exhibited ≈80% reduction in *Depdc5* mRNA levels compared to *Depdc5*^{Scr} (p<0,0007, Student's *t*-test; **Fig. 9B**), while Western Blotting analysis confirmed that a parallel reduction in Depdc5 protein was also present in *Depdc5*^{KD1} neurons (**Fig. 9C**; p=0.045, Student's *t*-test).

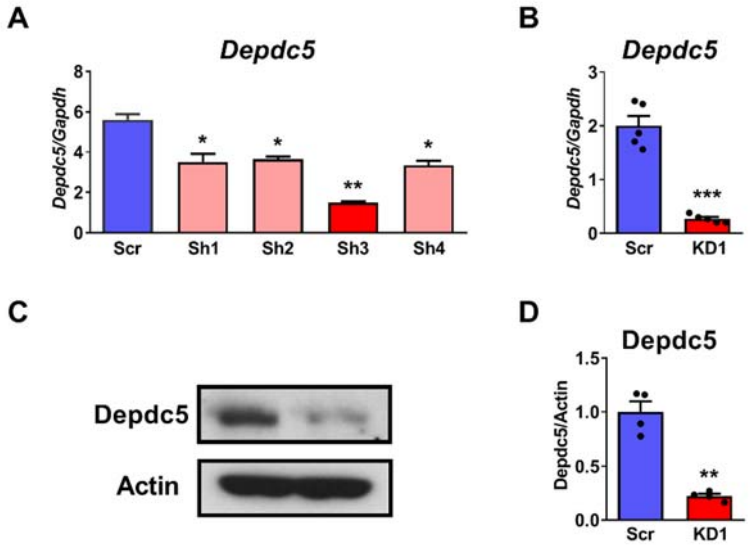

Figure 9: Characterization of shRNA-induced Depdc5 knockdown model.

A. *Histograms representing Depdc5 mRNA levels in HEK-293T cells after transfection with Sh1-4RNA against Depdc5 and Scramble control.* ***B****. Bar plots showing Depdc5 mRNA levels in* $Depdc5^{Scr}$ *and* $Depdc5^{KD1}$ *neurons, respectively.* ***C,D****. Representative Western Blot images* ***(C)*** *and bar plot* ***(D)*** *showing Depdc5 protein levels in* $Depdc5^{Scr}$ *and* $Depdc5^{KD1}$ *neurons. Data are expressed as means ± SEM. *p<0.05; **p<0.01; ***p<0.001, Student's t-test (B,D) and Kruskal-Wallis ANOVA/Dunn's test (A).*

5.5. Biochemical and morphological neuronal phenotype of chronic and acute Depdc5 deficiency

After validating our heterozygous and shRNA-induced models of Depdc5 deficiency, we characterized their neuronal phenotype to unmask the effects of Depdc5 loss-of-function at the cellular level. Firstly, we checked for the presence of a hyperactivation of mTORC1 pathway, by comparing the phosphorylated fraction of S6 protein of *Depdc5*$^{+/+}$ and *Depdc5*$^{+/-}$ primary cortical neurons with those of *Depdc5*^{KD1} and *Depdc5*^{Scr} by Western Blotting (**Fig. 10**). While constitutive *Depdc5*$^{+/-}$ neurons did not present an overt increase of pS6 compared to *Depdc5*$^{+/+}$ (n=5, p>0.05, Student's *t*-test), *Depdc5*^{KD1} neurons displayed an about 1.5-fold increase in pS6 levels with respect to *Depdc5*^{Scr} neurons (n=4, p=0.012, Student's *t*-test) (**Fig. 10A,B**). Since ectopic, pS6-positive enlarged neurons have been reported in FCD patients with *DEPDC5* loss-of-function, we immunostained neuronal cultures with the pS6 antibody (**Fig. 10C**). In agreement with biochemical analyses, only *Depdc5*^{KD1} neurons displayed an increased fluorescent intensity for pS6 (p=0.001, Student's *t*-test) without significant changes in the total S6 intensity, suggesting that the observed hyperphosphorylation of S6 is not due to an increased translation of the protein, but rather to its increased phosphorylation by mTORC1. Interestingly, we also observed a significant increase in soma size (≈15%; p=0.013, Student's *t*-test) in *Depdc5*^{KD1} neurons compared to *Depdc5*^{Scr}, confirming that mTORC1 hyperactivation triggers morphological changes *in vitro* (**Fig. 10D,E**). Overall, these results suggest that loss of heterozygosity in *Depdc5* is required to trigger the hyperactivation of the mTORC1 pathway and to induce morphological changes resembling those observed in patients with FCD.

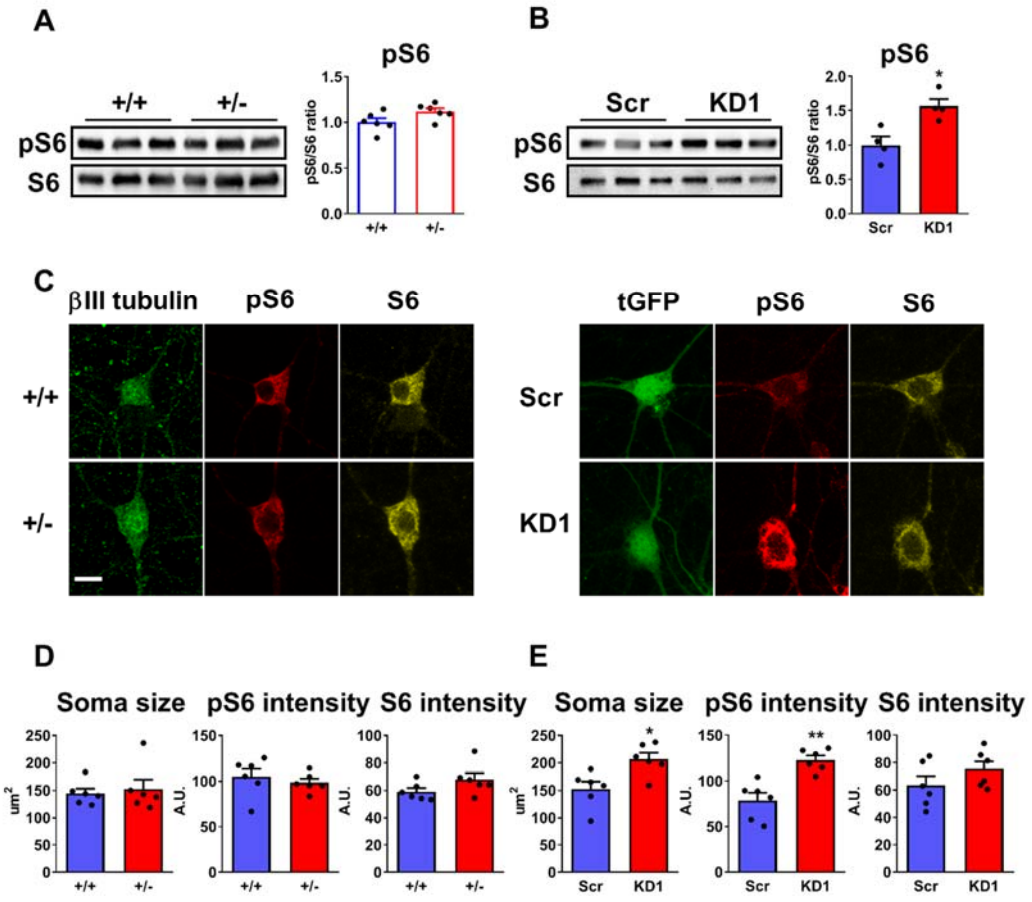

Figure 10: Acute Depdc5 deficiency induces hyperactivation of the mTORC1 pathway and cell body enlargement in primary cortical neurons.

A,B. *Representative western blot (left) and quantification (right) of the S6 phosphorylation levels (pS6) in Depdc5$^{+/+}$ and Depdc5$^{+/-}$ primary cortical neurons (**A**; n=6 embryos) and in Depdc5^{KD1} and Depdc5^{Scr} neurons. (**B**; n=4 independent preparations).* ***C.*** *Left: Representative confocal images of βIII-tubulin, pS6 and S6 staining in Depdc5$^{+/+}$ and Depdc5$^{+/-}$ neurons. Right: tGFP, pS6 and S6 immunofluorescence in Depdc5^{Scr} and Depdc5^{KD1} neurons, respectively.* ***D,E.*** *Bar plots showing the soma size (left) and the fluorescent intensity of pS6 (middle) and S6 (right) of primary cortical neurons from Depdc5$^{+/+}$ and Depdc5$^{+/-}$ mice (**D**; n=6 plates from 3 embryos per genotype) or of Depdc5^{Scr} and Depdc5^{KD1} neurons (**E**; n=6 plates from 3 independent preparations). Data are expressed as means ± SEM with individual experimental points. *p<0.05; ***p<0.001, Student's t-test. Scale bar: 10 µm.*

5.6. Increased complexity of dendritic arborization in Depdc5-deficient neurons

As stated in the introduction, mTORC1 plays a key role in dendrites and axons developments. To assess the potential neurodevelopmental changes due to Depdc5 downregulation, we next examined neurite elongation and branching by Sholl analysis in primary neurons prepared from *Depdc5*$^{+/+}$ and *Depdc5*$^{+/-}$ littermates, as well as in primary neurons nucleofected with either Scr or sh3 (**Fig. 11**). In *Depdc5*$^{+/-}$ neurons, the number of intersections was significantly higher than in *Depdc5*$^{+/+}$ neurons at distances between 90 and 110 μm from the cell body (**Fig. 11,B**). Accordingly, the area under the curve revealed a significant increase of neurite complexity for *Depdc5*$^{+/-}$ neurons compared to *Depdc5*$^{+/+}$ neurons (p=0.027, Student's *t*-test; **Fig. 11C**). The increased neurite arborization complexity was more pronounced in *Depdc5*^{KD1} neurons, with a much higher number of intersections at distances between 80 and 150 μm from the cell body, resulting in a significant increase in the area under the curve when compared to *Depdc5*^{Scr} neurons (p=0.017, Student's *t*-test; **Fig. 11D-F**). These results confirm that reduction of Depdc5 levels affects neuronal development by increasing the outgrowth and branching of neurites.

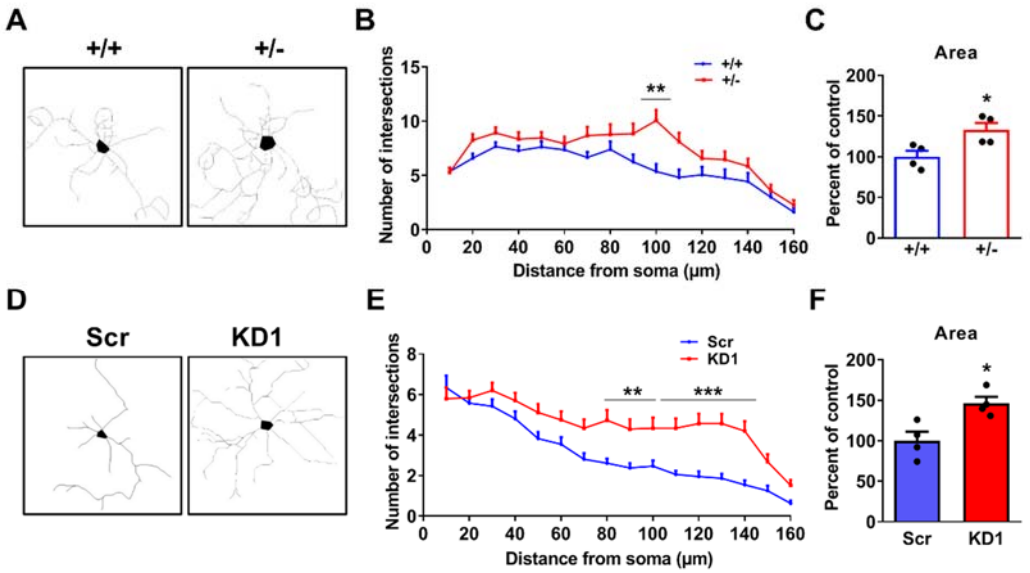

Figure 11: Depdc5-deficient neurons display an increased complexity of neurite arborization.

A-C. *Representative reconstructions of neuronal arborization of Depdc5$^{+/+}$ and Depdc5$^{+/-}$ cortical neurons (**A**), the respective Sholl analysis (**B**) and the histogram of the area under the curve (**C**) (N=4 embryos per genotype).* ***D-F.*** *Representative reconstruction of neuronal arborizations of Depdc5^{KD1} and Depdc5^{Scr} neurons. (**D**), the respective Sholl analysis (**E**) and the histogram of the area under the curve (**F**) (N=4 independent preparations). At least 10 neurons per preparation were analyzed. Data are expressed as means ± SEM with individual experimental points. *p<0.05; **p<0.001; ***p<0.001; Student's t-test (C,F) and ANOVA for repeated measures (B,E).*

5.7. Increased excitatory synaptic transmission in Depdc5-deficient neurons

The observed alterations due to Depdc5 loss of functions, especially regarding the increased dendrite arborization, open the possibility that other disturbances in related developmental processes, such as synaptic formation and homeostasis, are present in our mutants. Therefore, we investigated whether constitutive or acute Depdc5 deficiency could alter synaptic transmission *in vitro*. First, we focused on excitatory synaptic transmission. To study this aspect, we performed electrophysiological whole-cell recordings of mEPSCs in 14 DIV cortical neurons from *Depdc5*$^{+/+}$ and *Depdc5*$^{+/-}$ mice, as well as in 14 DIV *Depdc5*^{Scr} or *Depdc5*^{KD1}. (**Fig. 12A,B**). Interestingly, while no changes in frequency, amplitude and kinetics of mEPSCs were observed in *Depdc5*$^{+/-}$ neurons (**Fig. 12C,E**), *Depdc5*^{KD1} neurons showed a 4-fold increase in mEPSC frequency (p=0.0002, Student's *t*-test), together with significant increases in mEPSC amplitude (p=0.001, Mann-Whitney's *U*-test) and charge (p= 0.002, Student's *t*-test) with respect to *Depdc5*^{Scr} controls (**Fig. 12D,F**). *Depdc5*^{KD1} also showed an increased EPSC 10-90 rise time (p=0.046, Student's *t*-test) compared to *Depdc5*^{Scr} neurons, while the decay was not significantly affected (**Fig. 12E**). To ascertain whether the changes in mEPSC frequency were attributable to variations in synaptic density, we checked the distribution of excitatory synapses by confocal microscopy (**Fig 13A,B**). To investigate this aspect, we counted puncta that were double-labeled with an excitatory presynaptic marker, such as vGlut1, and an excitatory postsynaptic marker, such as Homer1, to unambiguous identify mature excitatory synapses. In agreement with the electrophysiological data, no changes in synaptic density were detected in *Depdc5*$^{+/-}$ neuronal networks with respect to *Depdc5*$^{+/+}$ cultures (**Fig. 13E,**

left), while a marked and significant increase in the density of excitatory synaptic synapses was observed in *Depdc5*^{KD1} neurons ($p<0.0001$, Student's *t*-test; **Fig. 13F,** *left*) that paralleled the increase in mEPSC frequency. To explain the observed changes in mEPSC amplitude and charge, the expression of the major AMPA receptor subunit GluA1 was investigated at Homer-positive puncta (**Fig. 13C,D**). While no changes in the GluA1 immunoreactivity were observed in *Depdc5*$^{+/-}$ neurons with respect to *Depdc5*$^{+/+}$ neurons (**Fig. 13E,** *right*), we found a significant increase in GluA1 fluorescence intensity in *Depdc5*^{KD1} neurons compared to *Depdc5*^{Scr} control neurons ($p=0.012$, Student's *t*-test; **Fig. 13F,** *right*).

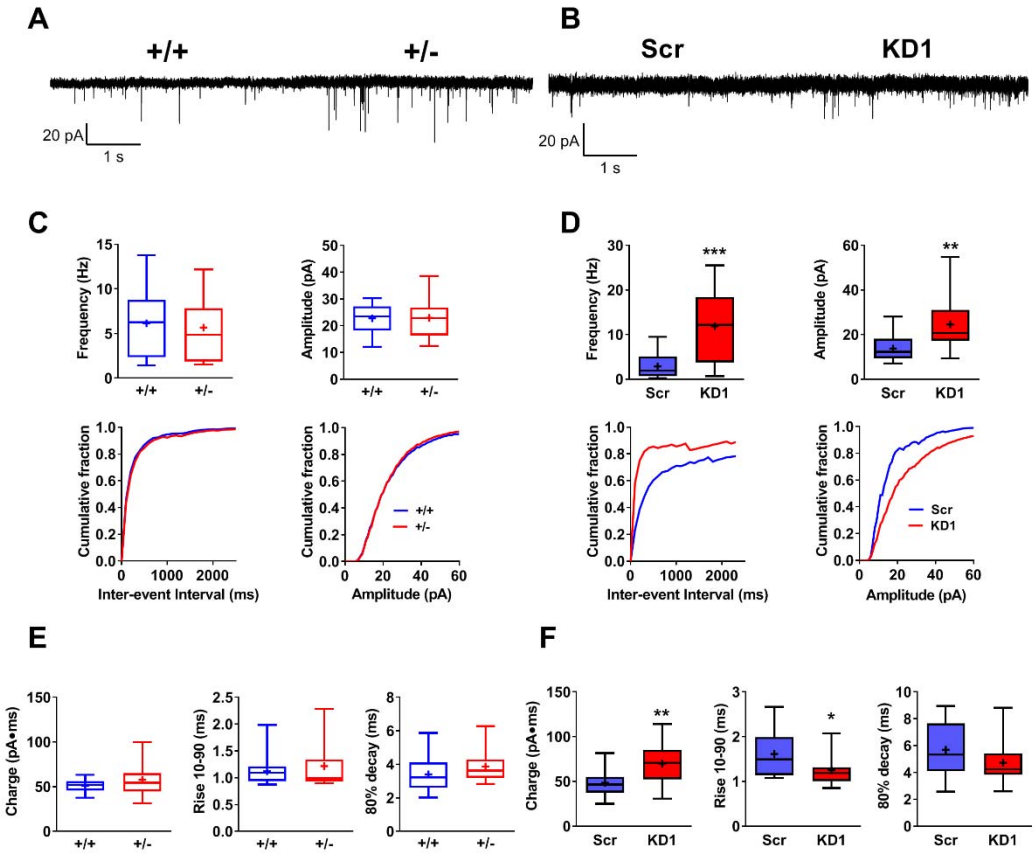

Figure 12: Acute Depdc5 silencing increases excitatory synaptic transmission.

A,B. *Representative traces of mEPSCs recorded in Depdc5$^{+/+}$ and Depdc5$^{+/-}$ primary cortical neurons (**A**) and in Depdc5^{KD1} and Depdc5^{Scr} neurons. (**B**).* ***C.*** *Mean frequency and amplitude of mEPSCs in Depdc5$^{+/+}$ (n=17) and Depdc5$^{+/-}$ (n=15) neurons (upper panels) and the respective mEPSC cumulative curves of inter-event interval and amplitude distributions (lower panels).* ***D.*** *Mean frequency and amplitude of mEPSCs in Depdc5^{Scr} (n=16) and Depdc5^{KD1} (n=19) neurons (upper panels) and the respective cumulative curves of mEPSC inter-event interval and amplitude distributions (lower panels).* ***E.*** *Box plots showing charge (left), 80% decay (middle) and 10-90 rise (right) of mEPSCs measured in Depdc5$^{+/+}$ and Depdc5$^{+/-}$ cortical neurons* ***F****. Box plots showing the same mEPSC parameters measured in Depdc5^{Scr} and Depdc5^{KD1} transduced WT neurons. All measurements were obtained from n=3 independent preparations. Data are expressed as box plots. *p<0.05; **p<0.01; ***p<0.001, Student's t-test/Mann Whitney's U-test.*

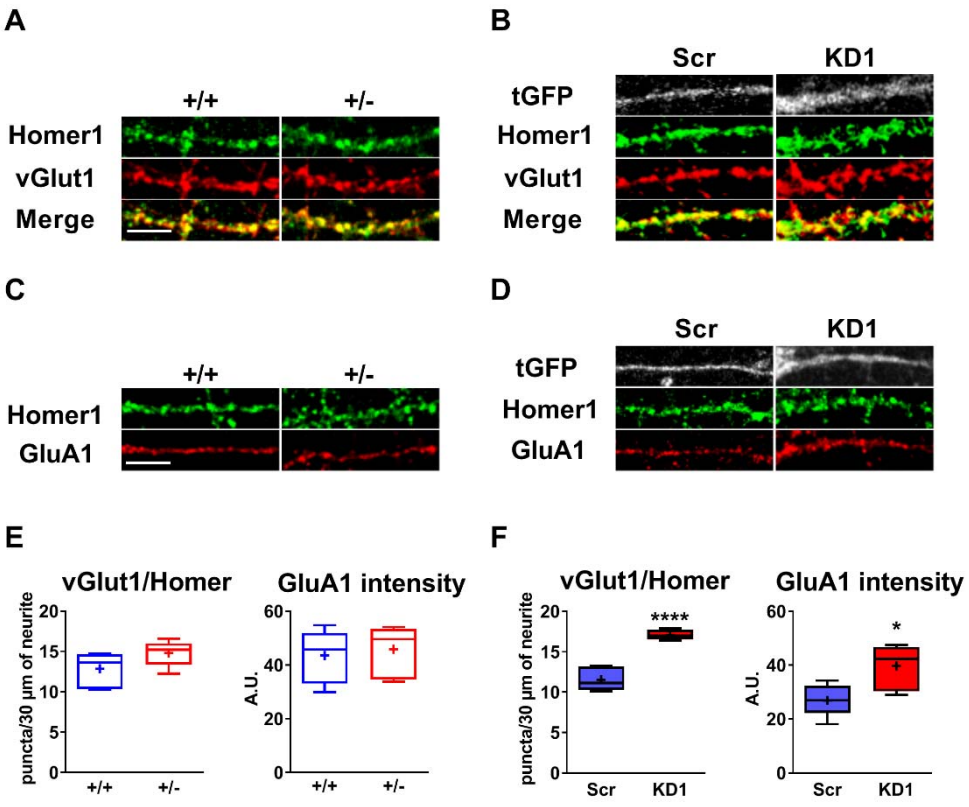

Figure 13: Increased number of excitatory synapses and AMPA receptor expression in neurons following acute Depdc5 silencing.

A,B *Representative confocal images of pre/post-synaptic markers vGlut1 and Homer1 in Depdc5$^{+/+}$ and Depdc5$^{+/-}$ neurons (**A**) and Depdc5^{Scr} and Depdc5^{KD1} neurons (**B**).* ***C,D.*** *Representative confocal images of the GluA1 AMPA receptor subunit at excitatory synaptic boutons in Depdc5$^{+/+}$ and Depdc5$^{+/-}$ neurons (**C**) and Depdc5^{Scr} and Depdc5^{KD1} neurons (**D**).* ***E****. Quantification of the linear density of excitatory synaptic boutons (left) and GluA1 AMPA receptor subunit fluorescent intensity (right) in Depdc5$^{+/+}$ and Depdc5$^{+/-}$ neurons.* ***F.*** *Quantification of the linear density of excitatory synaptic boutons (left) and GluA1 AMPA receptor subunit fluorescent intensity (right) in Depdc5^{Scr} and Depdc5^{KD1} neurons. All measurements were taken from 3 independent preparations. For histology, dendrites from at least 10 neurons per each preparation were analyzed. Data are expressed as box plots. *p<0.05; ****p<0.0001, Student's t-test/Mann Whitney's U-test. Scale bar: 10 µm.*

5.8. Inhibitory synaptic transmission is not markedly affected in Depdc5-deficient neurons

We next investigated whether Depdc5 deficiency could also alter inhibitory synaptic transmission in *Depdc5*$^{+/+}$ and *Depdc5*$^{+/-}$ neurons, as well as in *Depdc5*^{Scr} and *Depdc5*^{KD1} neurons (**Fig. 14A,B**). As observed for excitatory transmission, no detectable changes in mIPSC frequency, amplitude, charge or kinetics were observed under conditions of chronic haploinsufficiency in *Depdc5*$^{+/-}$ neurons **(Fig. 14C,E**). mIPSC frequency was neither affected after acute silencing of Depdc5, although we observed an increase in the amplitude of mIPSCs (p=0.015, Mann-Whitney's *U*-test; **Fig. 14D**). However, further analysis revealed that the overall charge of mIPSCs was unchanged, and that the effects on amplitude were attributable to an acceleration in mIPSC kinetics in *Depdc5*^{KD1} neurons that showed shortening of both the IPSC 10-90 rise time and 80% decay time (p=0.001 and 0.042, respectively, Student's *t*-test; **Fig. 14F**).. Immunocytochemical analysis of the density of inhibitory synapses identified by co-staining with the pre/postsynaptic inhibitory markers VGAT and Gephyrin, respectively, confirmed the electrophysiological results (**Fig. 15A,B**). Indeed, no differences were observed in synaptic density in both *Depdc5*$^{+/-}$ or *Depdc5*^{KD1} networks when compared to the respective controls, as assessed by double immunolabeling for vGAT and Gephyrin, a pre- and a post-synaptic marker of inhibitory synapses, respectively (**Fig. 15E,F,** *left*). Moreover, the expression of the $GABA_A$ β2 receptor subunit, measured as fluorescence intensity in Gephyrin-positive puncta, was not significantly changed in both *Depdc5*$^{+/-}$ and *Depdc5*^{KD1} neurons, confirming that the increase in mIPSC amplitude observed in *Depdc5*^{KD} neurons was not contributed by an increase in quantal size (**Fig. 15E,F,** *right*).

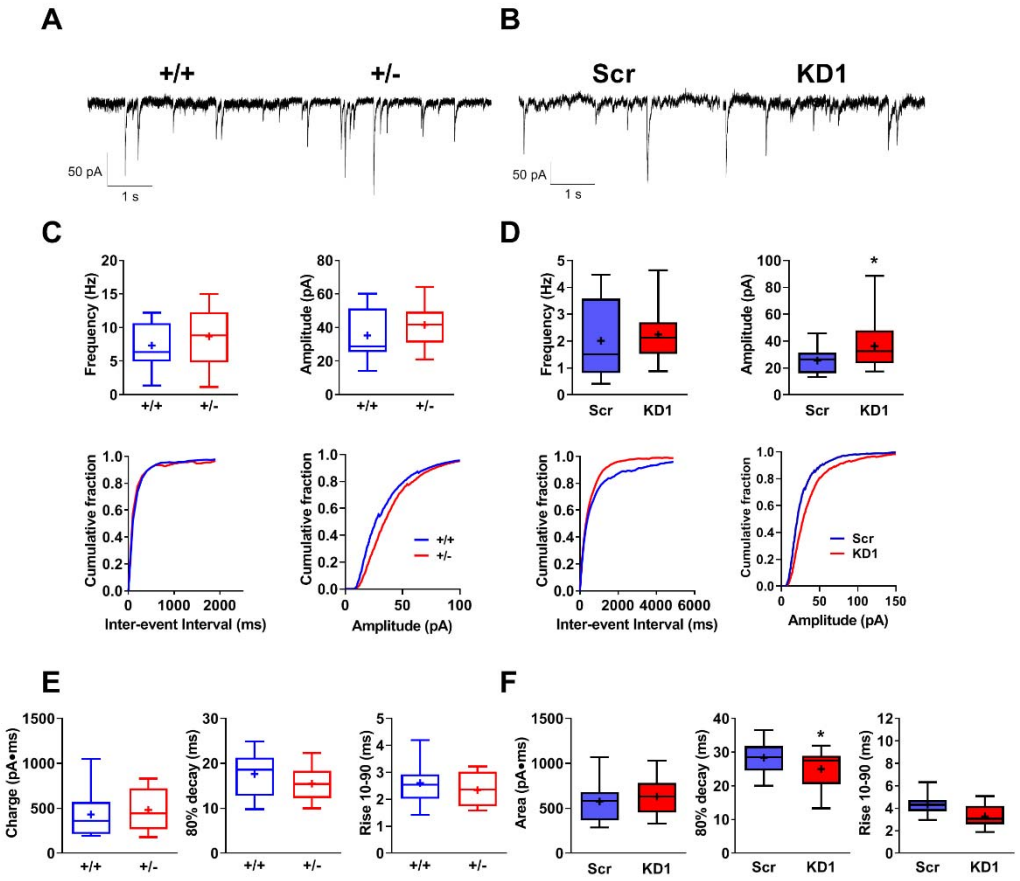

Figure 14. Acute Depdc5 silencing increases the amplitude, but not the frequency, of mIPSCs.

A,B. *Representative traces of mIPSCs recorded in Depdc5$^{+/+}$ and Depdc5$^{+/-}$ primary cortical neurons (**A**) and in Depdc5^{Scr} and Depdc5^{KD1} neurons (**B**).* ***C.*** *Mean frequency and amplitude of mIPSCs in Depdc5$^{+/+}$ (n=12) and Depdc5$^{+/-}$ (n=12) neurons (upper panels) and the respective cumulative curves of mIPSC inter-event interval and amplitude distributions (lower panels).* ***D.*** *Mean frequency and amplitude of mIPSCs in Depdc5^{Scr} (n=18) and Depdc5^{KD1} (n=18) neurons (upper panels) and the respective mIPSC cumulative curves of inter-event interval and amplitude distributions (lower panels).* ***E.*** *Box plots showing charge (left), 80% decay (middle) and 10-90 rise (right) of mIPSCs measured in Depdc5$^{+/+}$ (n=12) and Depdc5$^{+/-}$ (n=12) cortical neurons* ***D.*** *Box plots showing the same mIPSC parameters measured in Depdc5^{Scr} (n=18) and Depdc5^{KD} (n=18) transduced WT neurons. All measurements were obtained from n=3 independent preparations. Data are expressed as box plots. *p<0.05, **p<0.01, Student's t-test.*

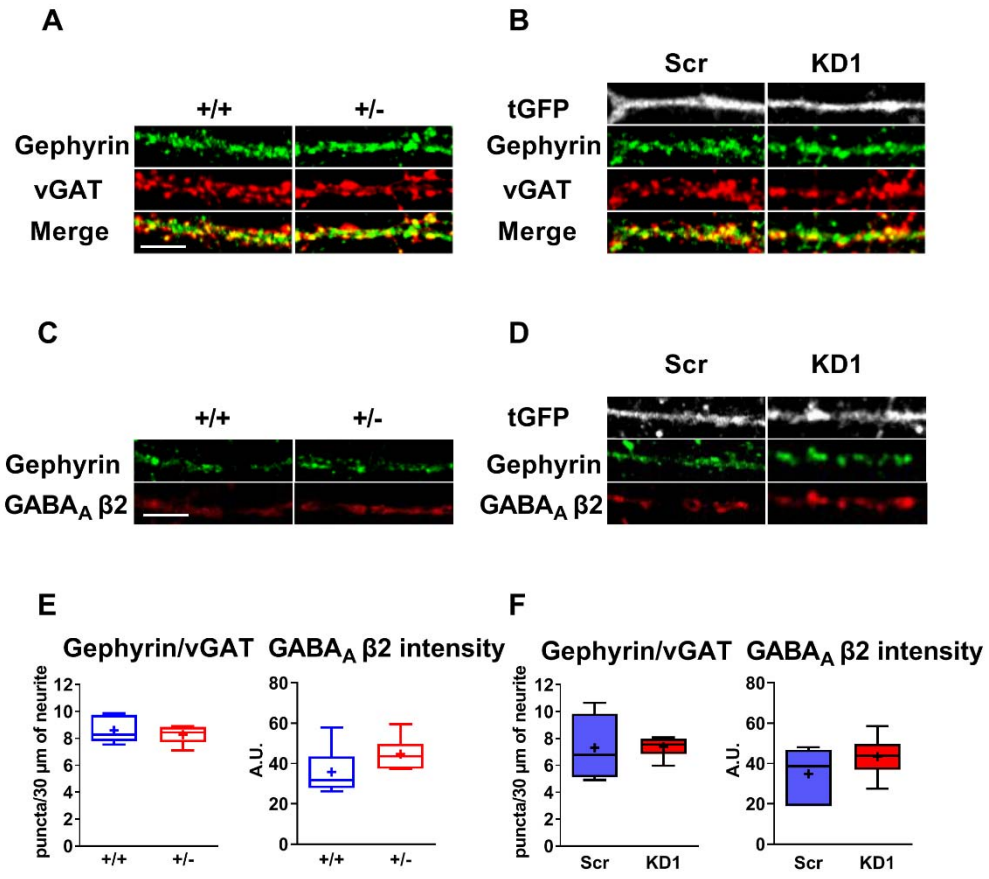

Figure 15: Depdc5 deficiency does not alter the density of inhibitory synapses and the postsynaptic expression of the GABA$_A$ β2 receptor subunit.

A,B. *Representative confocal images of pre/post-synaptic markers vGAT and Gephyrin in Depdc5$^{+/+}$ and Depdc5$^{+/-}$ neurons (**A**) and Depdc5^{Scr} and Depdc5^{KD1} neurons (**B**).* ***C,D.*** *Representative confocal images of GABA$_A$ β2 receptor subunit at excitatory synaptic boutons in Depdc5$^{+/+}$ and Depdc5$^{+/-}$ neurons (**C**) and Depdc5^{Scr} and Depdc5^{KD1} neurons (**D**).* ***E.*** *Quantification of the linear density of inhibitory synaptic boutons (left) and GABA$_A$ β2 receptor subunit fluorescent intensity (right) in Depdc5$^{+/+}$ and Depdc5$^{+/-}$ neurons.* ***F.*** *Quantification of the linear density of inhibitory synaptic boutons (left) and GABA$_A$ β2 receptor subunit fluorescent intensity (right) in Depdc5^{Scr} and Depdc5^{KD1} neurons. All measurements were taken from 3 independent preparations. For histology, dendrites from at least 10 neurons per each preparation were analyzed. Data are expressed as box plots. Scale bar: 10 µm.*

5.9. Synaptic ultrastructure is not altered by Depdc5 deficiency

Although the electrophysiological phenotype suggested that an increase in synapse number, rather than a change in the quantal properties of synaptic transmission, was responsible for the increased excitatory strength, we checked whether Depdc5 deficiency had any effect on synaptic ultrastructure in *Depdc5*$^{+/+}$ and *Depdc5*$^{+/-}$ neurons (**Fig. 16A**), as well as in *Depdc5*^{Scr} and *Depdc5*^{KD1} neurons (**Fig. 16B**). Therefore, we performed a detailed morphometric analysis of synaptic contacts by TEM. The analysis failed to detect major changes in synaptic ultrastructure. Indeed, both *Depdc5*$^{+/-}$ and *Depdc5*^{KD1} neurons showed no significant changes in nerve terminal area, active zone (AZ) length, number and density of total nerve terminal synaptic vesicles (SVs) and number and linear density of docked SVs, as compared to the respective controls (**Fig. 16C,D**). However, a significant increase ($p = 0.0211$, Mann-Whitney's *U*-test) in the mean area, but not in the number, of endosomes was observed in *Depdc5*^{KD1} nerve terminals, suggesting the presence of an impaired autophagic flux (**Fig. 16E,F**).

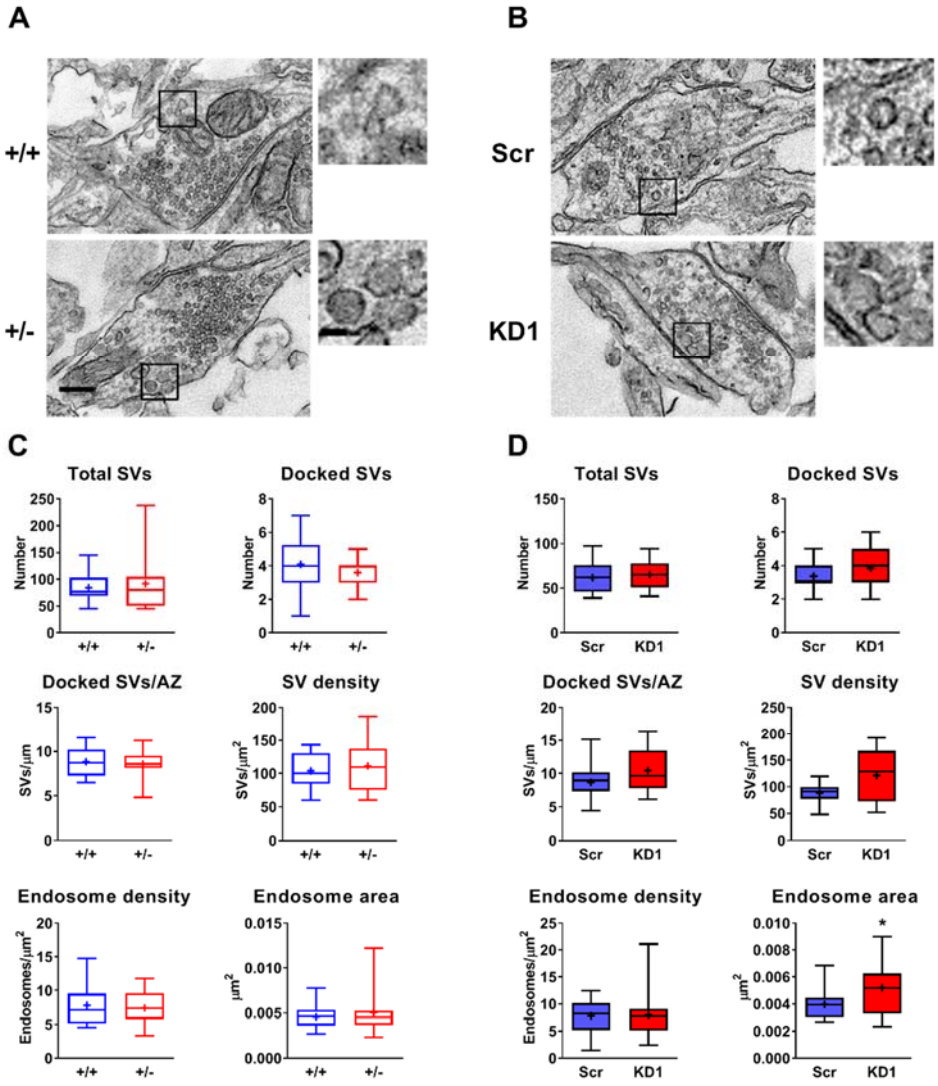

Figure 16. Acute Depdc5 silencing increases the size of nerve terminal endosomes without affecting synaptic ultrastructure.

A,B. *Representative TEM micrographs showing synaptic morphology of Depdc5$^{+/+}$ and Depdc5$^{+/-}$ primary neurons (**A**), and Depdc5^{Scr} and Depdc5^{KD1} neurons (**B**).* ***C,D.*** *Histograms showing morphometric analysis of synapses from Depdc5$^{+/+}$ and Depdc5$^{+/-}$ neurons (**C**) and Depdc5^{Scr} and Depdc5^{KD1} neurons (**D**) for the following parameters: total SV number, SV density, docked SV number, docked SV density, endosome density and mean endosome area. Nerve terminal areas (means ± SEM) were: Depdc5$^{+/+}$, 0.811 ± 0.211; Depdc5$^{+/-}$, 0.832 ± 0.397; Depdc5^{Scr}, 0.741 ± 0.280; Depdc5^{KD1}, 0.652 ± 0.219. AZ lengths (means ± SEM) were: Depdc5$^{+/+}$, 0.496 ± 0.142; Depdc5$^{+/-}$, 0.427 ± 0.104; Depdc5^{Scr}, 0.410 ± 0.110; Depdc5^{KD1}, 0.367 ± 0.064. All measurements were taken from 3 independent preparations. At least 10 synapses per each preparation were analyzed. Data are expressed as box plots. *p<0.05, Student's t-test. Scale bars: 0.2 µm and 0.05 µm (zoomed pictures).*

5.10. Acute Depdc5-deficiency increases intrinsic excitability of principal neurons

We next investigated whether Depdc5 downregulation was associated with an increase in intrinsic excitability, in addition to the observed excitatory/inhibitory synaptic imbalance. We thus performed electrophysiological recordings in current-clamp configuration to evaluate the passive and active properties of single cortical neurons from *Depdc5*$^{+/+}$ and *Depdc5*$^{+/-}$ mice or of WT neurons that had been subjected to RNA interference to silence Depdc5 expression (**Fig. 17A,B**). No major changes in excitability were observed from the firing rate *versus* injected current curves between *Depdc5*$^{+/-}$ and *Depdc5*$^{+/+}$ neurons, in both mean firing frequency (number of APs elicited during the 500 ms of current injection), instantaneous firing frequency and rheobase (**Fig. 17C, Table 1**). Similarly, no changes were observed in the basic passive properties, as well as in the threshold voltage, and AP shape parameters obtained from the phase-plane plot analysis (**Table 1**). On the contrary, *Depdc5*^{KD1} neurons displayed a significant increase in the mean firing frequency at higher levels of injected current compared to *Depdc5*^{Scr} neurons that was paralleled by a significant decrease in the rheobase (**Fig. 8D, Table 1**). *Depdc5*^{KD1} neurons did not exhibit altered passive properties. However, the analysis of the AP waveform by phase-plane plot analysis showed significant increases in the maximum rising and repolarization slopes and AP peak (**Table 1**), consistent with a condition of hyperexcitability induced by the acute Depdc5 depletion.

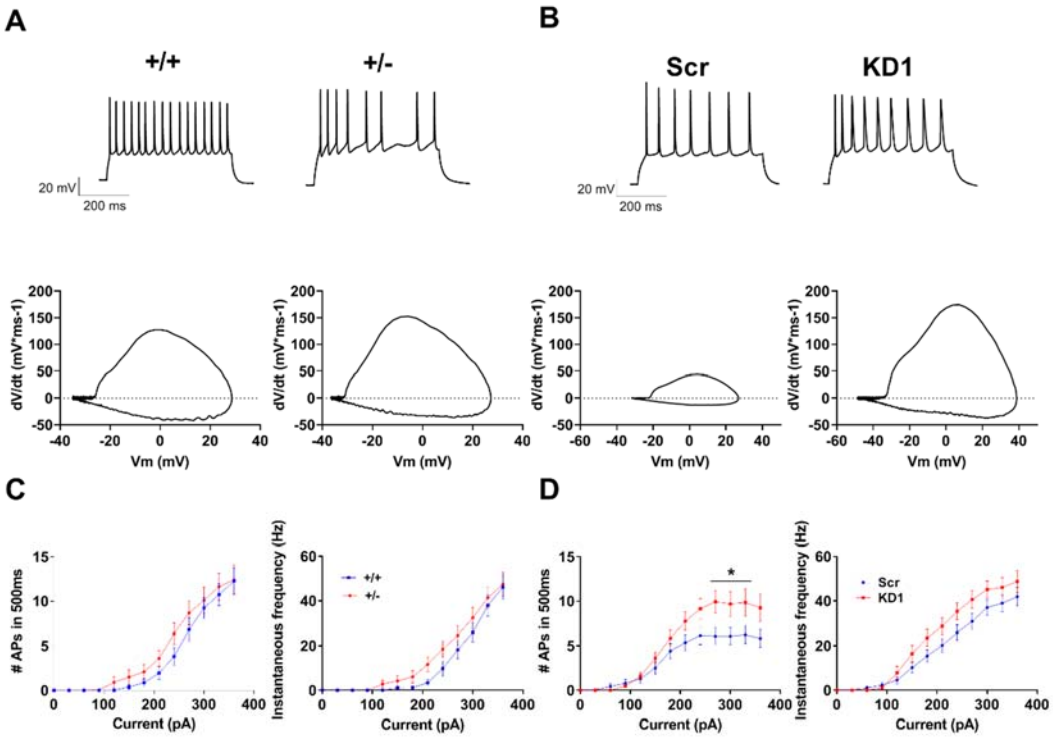

Figure 17: Acute Depdc5 silencing increases intrinsic excitability.

A,B. *Representative recordings of action potentials induced by the injection of 280 pA for 500 ms (upper panels) and representative phase-plane plots of the first action potential in the train (lower panels) in Depdc5$^{+/+}$ and Depdc5$^{+/-}$ neurons (**A**) and in Depdc5^{Scr} and Depdc5^{KD1} neurons (**B**).* ***C.*** *Mean number of APs evoked by the 500 ms current step in Depdc5$^{+/+}$ (n=22) and Depdc5$^{+/-}$ (n=22) primary neurons (left) and instantaneous frequency of APs (right).* ***D.*** *Mean number of APs evoked by the 500 ms current step in Depdc5^{Scr} (n=40) and Depdc5^{KD1} (n=31) neurons (left) and instantaneous frequency of APs (right). All measurements were taken from 3 independent preparations. Data are expressed as means ± SEM. *p<0.05; ANOVA for repeated measures.*

Table 1. **Passive and active properties of Depdc5-deficient primary cortical neurons.**

Parameters	*Depdc5*$^{+/+}$	*Depdc5*$^{+/-}$	p	*Depdc5*^{Scr}	*Depdc5*^{KD1}	p
V_{rest} *(mV)*	- 53.41 ± 1.55 (n=22)	- 52.55 ± 1.42 (n=22)	0,68	- 53.00 ± 1.39 (n=40)	- 50.84 ± 2.11 (n=31)	0.39
C_{in} *(pF)*	40.97 ± 3.39 (n=25)	34.91 ± 1.79 (n=27)	0.28	51.88 ± 4.97 (n=14)	42.92 ± 3.82 (n=19)	0.16
R_{in} *(MΩ)*	201.8 ± 16.25 (n=22)	208.1 ± 17.48 (n=22)	0.79	264.4± 15.28 (n=40)	255.2 ± 15.00 (n=31)	0.84
Rheobase (pA)	213.6±9.03 (n=22)	198.2±11.89 (n=22)	0.30	160.3 ± 10.26 (n=40)	133.5 ± 7.80 (n=31)	0.04*
V_{thr} *(mV)*	- 30.46 ± 1.69 (n=22)	- 29.61 ± 1.54 (n=22)	0.71	- 28.61 ± 1.04 (n=40)	- 29.99 ± 1.13 (n=31)	0.37
Max rising slope (mV/ms)	101.4 ± 7.3 (n=22)	119.8 ± 14.2 (n=22)	0.74	67.16 ± 6.85 (n=40)	95.89 ± 11.16 (n=31)	0.04*
Half-width (ms)	1.69 ± 0.12 (n=22)	1.42 ± 0.10 (n=22)	0.31	2.71 ± 0.23 (n=40)	2.101 ± 0.13 (n=31)	0.17
AP peak (mV)	25.17 ± 2.20 (n=22)	27.07 ± 2.27 (n=22)	0.55	22.70 ± 1.73 (n=40)	30.29± 2.63 (n=31)	0.02*
Max repol. slope (mV/ms)	- 28.57 ± 1.96 (n=22)	- 32.29 ± 2.69 (n=22)	0.27	- 20.14 ± 1.73 (n=40)	- 26.50 ± 3.11 (n=31)	0.09
Phase slope (ms^{-1})	10.45±0.71 (n=22)	10,55±0,65 (n=22)	0.92	7.201±0,48 (n=40)	8.705±0.69 (n=31)	0.22

Data are expressed as means ± SEM. The number of replicates is indicated. *p<0.05; **p<0.01; Student's *t*-test/Mann-Whitney's *U*-test.

5.11. Depdc5 knockdown with an alternative shRNA resumes most of the *Depdc5*^{KD1} neurons phenotype

To confirm that the observed phenotype in *Depdc5*^{KD1} neurons was specifically due to the knockdown of *Depdc5* and to exclude any off-target effect of the sh3 construct, we cloned and alternative shRNA, the sh4, in a lentiviral vector and used for experiments in primary neurons. qRT-PCR and Western Blot analysis showed that sh4-transduced neurons (*Depdc5*^{KD2}) exhibited 45% reduction of *Depdc5* mRNA and ≈ 40% reduction of Depdc5 protein level compared to *Depdc5*^{Scr} (**Fig. 18A,B**; p=0.028 and p=0.0285, respectively; Mann-Whitney's *U*-test/Student's *t*-test). *Depdc5*^{KD2} neurons displayed a ≈ 30% increase of the phosphorylated fraction of S6 protein (**Fig. 18C**; p=0.044; Student's *t*-test), suggesting that an acute depletion of about half Depdc5 protein level is sufficient to induce hyperactivation of the mTORC1 pathway. Similarly to *Depdc5*^{KD1} neurons, immunofluorescence analysis showed that *Depdc5*^{KD2} exhibited an increase in soma size and pS6 immunoreactivity compared *Depdc5*^{Scr}, with no changes in the intensity of total S6 protein (**Fig. 18D,E**; p=0.007 and p=0.004, respectively; Student's *t*-test). We then recorded mEPSCs and firing activity to assess the synaptic phenotype of *Depdc5*^{KD2} neurons. Similar to the sh3-mediated silencing, we observed an increase in the frequency of mEPSCs of *Depdc5*^{KD2} neurons compared to the control (**Fig. 18G**; p=0.0001, Mann-Whitney's *U*-test), in the absence of significant changes in amplitude of miniature events. The same result was observed for both mean firing frequency and instantaneous firing frequency, where no differences between *Depdc5*^{KD2} and *Depdc5*^{Scr} neurons were observed (**Fig. 18I**).

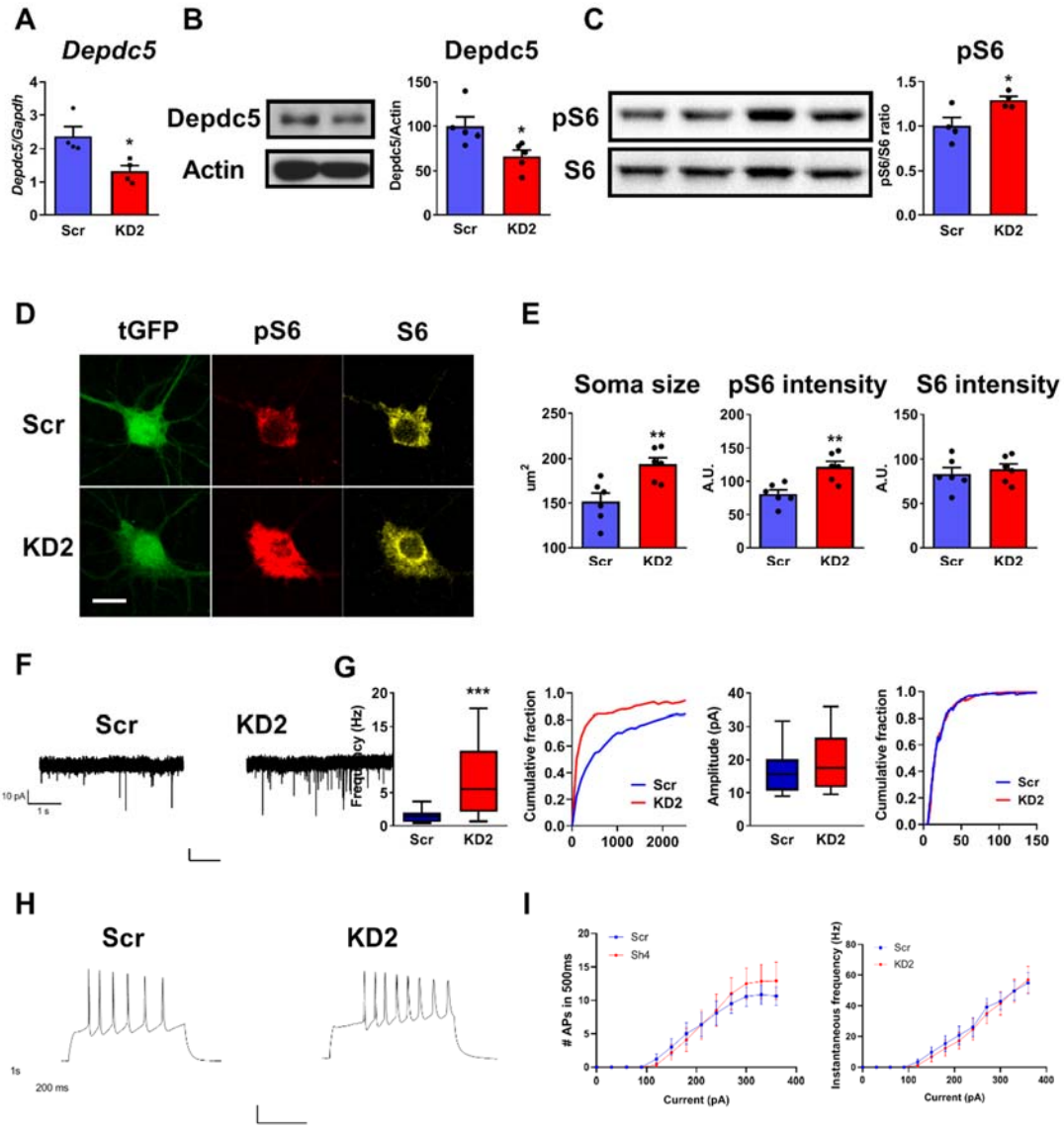

Figure 18: Depdc5^{Kd2} neurons recapitulate most of the phenotype of Depdc5^{Kd1} neurons. *A. Depdc5 mRNA levels in Depdc5^{KD2} and Depdc5^{Scr} neurons.* ***B,C.*** *Representative Western Blot images (left) and bar plot (right) showing the level of Depdc5 protein* ***(B)*** *and the phosphorylated fraction of S6 protein* ***(C)*** *in Depdc5^{KD2} and Depdc5^{Scr} neurons.* ***D,E.*** *Representative Western Blot images* ***(D)*** *and bar plot showing the soma size (left) and the fluorescent intensity of pS6 (middle) and S6 (right) in Depdc5^{KD2} and Depdc5^{Scr} neurons.* ***F.*** *Representative traces of mEPSCs recorded from Depdc5^{Scr} and Depdc5^{KD2}.* ***G.*** *Box plot showing mEPSCs frequency and amplitude recorded in Depdc5^{KD2} and Depdc5^{Scr} with the respective cumulative distributions.* ***H.*** *Representative recordings of action potentials in Depdc5^{Scr} and Depdc5^{KD2} neurons,* ***I.*** *Mean number of APs evoked by the 500 ms current step in Depdc5^{Scr} and Depdc5^{KD2} neurons (left) and instantaneous frequency of APs (right). All measurements were taken from 3 independent preparations. Data are expressed as box plots and as means ± SEM.***p<0.001, Mann Whitney's U-test. Scale bar: 10 µm.*

6. Discussion

DEPDC5 mutations are emerging as a common cause of a broad epileptic syndrome spectrum (Poduri, 2014; Baldassari et al., 2019a; Baldassari et al., 2019b;), including FCD, that are characterized by dysmorphic neurons displaying enhanced mTOR activation (for reviews see Marsan and Baulac, 2018; Iffland and Crino, 2017). Notwithstanding Depdc5 has been identified as a part of the GATOR1 complex (Bar-Peled et al., 2013), its neuronal profile is still poorly characterized. mTORC1 plays a key role in neurons soma growth, dendritic branching and synaptogenesis, and synaptic excitability (Laplante and Sabatini, 2012; Lasarge and Danzer, 2014). We therefore investigated these aspects in primary neuron cultures from either heterozygous *Depdc5*$^{+/-}$ mice or in primary neurons silenced for Depdc5 by RNA interference.

It was previously reported that heterozygous *Depdc5*$^{+/-}$ mice failed to replicate the main hallmarks of the human pathology, such as spontaneous seizures (Marsan et al., 2016; Hughes et al., 2017). Here we demonstrate that, although *Depdc5*$^{+/-}$ mice have a reduced epileptic threshold to PTZ, they do not display alterations in the mTORC1 pathway and in cortical cytoarchitecture. Moreover, primary heterozygous neurons do not exhibit overt alterations of mTORC1 signaling and, except for a slightly increased dendritic tree development, soma size, synaptogenesis and synaptic transmission were comparable to WT neurons.

Strikingly, acute silencing of *Depdc5* in WT neurons by RNA interference revealed that a ≈ 80% decrease in *Depdc5* mRNA is able to induce morphological defects that resemble those seen in patients with FCD consisting of mTOR hyperactivated enlarged neurons. Recent studies showed the occurrence of second-hit *DEPDC5* variants in resected brain samples from individuals with FCD (Baldassarri et al. 2019, Sim et al., 2019). This variant was present only in abnormal neurons within the dysplastic area

and the somatic mutation load correlates with dysmorphic cell density (Sim et al., 2019). Our experiments, in line with these findings, highlight the importance of loss of heterozygosity to trigger the changes in neuronal morphology and connectivity that, together with the impairment in neuronal differentiation and migration associated with mTOR hyperactivity, could possibly lead to macroscopic dysplasia. Our results also suggest an important neurodevelopmental role of *DEPDC5*. Indeed, acutely depleted neurons displayed both an increased complexity of neuritic arborization and altered synaptogenesis, processes in which the role of mTOR in well established (Hoeffer and Klann, 2010). Moreover, *Depdc5*^{KD2} neurons, whose Depdc5 depletion level was comparable to *Depdc5*$^{+/-}$ neurons, displayed most of the alterations observed in *Depdc5*^{KD1}, including hyperactivation of mTORC1 pathway, increased soma size and increased frequency of mEPSCs, that were absent in heterozygous neurons. The less intense, but still severe, phenotype observed in *Depdc5*^{KD2} neurons suggests that also the acute deletion of *Depdc5* plays a role in the establishment of the Depdc5-related phenotype.

It is not clear, however, why the acute loss of 40% of Depdc5 in neurons generates a severe phenotype that is absent in constitutive heterozygous neurons. It has been reported that negative feedback from phosphorylated S6 to Akt could limit mTORC1 hyperactivation under conditions of constitutive mTORC1 stimulation, such as chronic insulin exposure (Howell and Manning, 2011). Future studies are needed to address if the acute loss of Depdc5 could overcome this feedback. This would be particularly important due to the dramatic phenotype given by somatic mutation of *DEPDC5.*

In our models the synaptogenesis defect appears to affect only excitatory synapses, while inhibitory synapses develop normally. The greatly increased frequency and amplitude of mEPSCs, paralleled by increased density of excitatory synapses and expression of glutamate receptors, may generate an excitation/inhibition imbalance that

triggers epileptogenesis. These results differ from previous data in the zebrafish, where *Depdc5* knockout was associated with deficits in the GABAergic systems (Swaminathan et al., 2018). Although this discrepancy could be due to the time-course of Depdc5 silencing or to species-specific differences, the overall result will be an E/I imbalance in both experimental models.

Recently, it has been shown that *Depdc5* mosaic knockout leads to growth of abnormal dendritic tree, increased amplitude of sEPSPs and local hyperexcitability of pyramidal neurons (Ribierre et al., 2018; Hu et al., 2018). Our data confirm these findings, suggesting that the hyperactivation of cortical networks can result from both increased number of excitatory synaptic connections and increased expression of postsynaptic excitatory receptors, leading to increased excitatory strength. The *Depdc5*-linked epileptogenic phenotype is also contributed by an increase in the intrinsic excitability and an enhancement of AP dynamics, partially consistent with what observed following mosaic inactivation of mouse *Depdc5* by in utero electroporation (Ribierre et al., 2018). Indeed, in the latter, pyramidal neurons display a reduced firing frequency and no differences in the frequency of spontaneous events. However, the large increase in cell capacitance displayed by electroporated neurons, that is absent in *Depdc5*^{KD1} neurons, could account for the reduced firing pattern; this, in turn, could possibly influence the reduced frequency of spontaneous events. In any case, the significantly higher gain of firing frequency (slope of the F-I curve) above threshold of electroporated *Depdc5* knockout neurons is consistent with an increased intrinsic responsiveness to current injection and strongly suggests an increase in the excitability properties of pyramidal neurons *in-vivo*. Differences in the model systems, and compensatory effects arising after chronic knockdown could be, at least partially, responsible for the observed differences and further studies are needed to clarify this point.

Our results indicate that the hyperactivity of the mTOR pathway has combined effects at ion channel and synaptic levels that predominantly affect excitatory neurons, thereby leading to a severe imbalance between excitatory and inhibitory activity. Electrophysiological recording of human neurons from TS pediatric patients presenting FCD revealed that spontaneous GABA synaptic activity was increased compared to glutamate activity (Cepeda et al., 2005). Pacemaker GABA activity, consisting of rhythmic synaptic events, was also frequently observed in FCD cases (Cepeda et al., 2014). In addition, similar to cytomegalic pyramidal neurons, cytomegalic GABAergic interneurons are hyperexcitable and display spontaneous membrane depolarizations and bursting activity, making them potential generators of epileptic activity (Fauser et al., 2013). However, also GluA2/3 subunits of AMPA receptor and metabotropic glutamate receptors (particularly mGluR1 and mGluR5) are highly expressed in dysplastic neurons (Babb et al., 1998; Hilbig et al., 1999; Aronica et al., 2003), suggesting that an increased excitatory drive is also present *in-vivo*. Overall, these results indicate that human brain samples of FCD display a condition of hyperexcitability, at least in a subset of neurons, which is a constant finding in both experimental models of TS and patients' brain tissues and, therefore, could be regarded as a common denominator of mTOR-related FCDs.

The molecular mechanism underlying these defects and their specificity for excitatory neurons in our model is still unclear. mTOR signaling has an important role in regulating the autophagy flux (Hall, 2008; Hosokawa et al., 2009; Jung et al., 2009; Kim et al., 2011; Yu et al., 2010). Autophagy is a homeostatic process that involves the turnover of intracellular organelles and proteins through the endolysosomal system (Glick et al., 2010). Recently, it has been shown that deficiency in mTOR-mediated autophagy could reduce synaptic pruning (Tang et al., 2014; Kim et al., 2017). Moreover, another report suggests that autophagy mediates the internalization of

glutamate receptors after chemical long-term depression (Shehata et al., 2012). Indeed, the enlargement of nerve terminal endosomes, consistent with the synaptic defects observed after acute *Depdc5* silencing, could be mediated, at least in part, by a defective autophagy following mTOR hyperactivation. This is also in line with recent studies suggesting autophagy impairment in neurons from tuberous sclerosis complex (McMahon et al., 2012; Miyahara et al., 2013) and, more generally, in a wide spectrum of epileptic encephalopathies (Yasin et al., 2013; Park et al., 2018; Fassio et al., 2018).

7. Conclusions and future perspectives

Overall, the data presented in this dissertation indicate that the acute, but not the constitutive, Depdc5 knockdown leads to a solid neuronal phenotype that is reminiscent of the somatic second-hit mechanism in patients with FCD (Ribierre et al., 2018). Indeed, growing evidences suggest that *DEPDC5* somatic mutations are present in dysmorphic neurons and could be necessary to trigger FCD with mTOR hyperactivation. The data uncover a novel synaptic phenotype resulting from Depdc5 knockdown and mTOR hyperactivity with increased excitatory strength and excitatory/inhibitory imbalance, highlighting the epileptogenic potential of its deficiency. In future experiments, we are planning to characterize short- and long-term plasticity of excitatory and inhibitory synapses in neurons lacking Depdc5, to assess the potential contribution of altered plasticity to the epileptogenic process.

The severe neural phenotype observed after acute and pronounced Depdc5 knockdown supports the idea that loss of heterozygosity, and thereby significant loss of inhibitory brake on mTOR is necessary for the establishment of DEPDC5-related FCD. Our results also uncover an important developmental role for DEPDC5, showing for the first time that its acute deletion leads to morpho-functional alterations that are absent in chronic haploinsufficient neurons. Our future experiments in this direction will be aimed at clarifying the importance of the developmental loss of Depdc5 in the pathogenic process.

Taken together, our results represent new insight into the Depdc5-related epileptogenic process and represent a starting point for further investigations aimed at identifying new targets for alternative therapeutic strategies for GATOR1-related neurological disorders.

8. Acknowledgements

Undertaking this PhD has been a truly life-changing experience for me and it would not have been possible to do without the support that I received from many people.

In the first place, I thank my supervisor Professor Fabio Benfenati for his special mentoring and supervision, and the help he gave me to develop this project.

I want to acknowledge Dr. Stephanie Baulac and Dr. Alfonso Represa for their usefull comments concerning this manuscript.

I thank Maria Sabina Cerullo for electrophysiological recordings and precious discussions, Dr. Caterina Michetti for the help in in-vivo experiments and Dr. Antonella Marte for biochemical assays.

I thank Dr. Enrico Castroflorio for his valuable supervision during my training on EM techniques.

A special mention goes to my fellow PhD students Matteo Moschetta, Assia Merolla, Carmela Vitale and Giulio Alberini for all the constructive discussions and the funny moments we shared inside and outside the lab, and of course to all the people working at NSYN.

I am indebted to my beloved Annalisa for her infinite love, support and patience. Without you on my side, nothing of this would have been possible, and everything would have been meaningless: you will always be in my heart.

Lastly, I would like to express my genuine gratitude to my parents and my brother for their support and never-ending love.

9. References

Antion MD, Merhav M, Hoeffer CA, Reis G, Kozma SC, Thomas G, Schuman EM, Rosenblum K, Klann E. Removal of S6K1 and S6K2 leads to divergent alterations in learning, memory, and synaptic plasticity. Learn Mem. 2008 Jan 3;15(1):29-38. doi: 10.1101/lm.661908.

Aronica E, Crino PB. Epilepsy related to developmental tumors and malformations of cortical development. Neurotherapeutics. 2014 Apr;11(2):251-68. doi: 10.1007/s13311-013-0251-0. Review.

Aronica E, Gorter JA, Jansen GH, van Veelen CW, van Rijen PC, Ramkema M, Troost D. Expression and cell distribution of group I and group II metabotropic glutamate receptor subtypes in taylor-type focal cortical dysplasia. Epilepsia. 2003 Jun;44(6):785-95.

Avruch J, Hara K, Lin Y, Liu M, Long X, Ortiz-Vega S, Yonezawa K. Insulin and amino-acid regulation of mTOR signaling and kinase activity through the Rheb GTPase. Oncogene. 2006 Oct 16;25(48):6361-72.

Babb TL, Ying Z, Hadam J, Penrod C. Glutamate receptor mechanisms in human epileptic dysplastic cortex. Epilepsy Res. 1998 Sep;32(1-2):24-33.

Baldassari S, Licchetta L, Tinuper P, Bisulli F, Pippucci T. GATOR1 complex: the common genetic actor in focal epilepsies. J Med Genet. 2016 Aug;53(8):503-10. doi: 10.1136/jmedgenet-2016-103883.

Baldassari S, Picard F, Verbeek NE, van Kempen M, Brilstra EH, Lesca G, Conti V, Guerrini R, Bisulli F, Licchetta L, Pippucci T, Tinuper P, Hirsch E, de Saint Martin A, Chelly J, Rudolf G, Chipaux M, Ferrand-Sorbets S, Dorfmüller G, Sisodiya S, Balestrini S, Schoeler N, Hernandez-Hernandez L, Krithika S, Oegema R, Hagebeuk E, Gunning B, Deckers C, Berghuis B, Wegner I, Niks E, Jansen FE, Braun K, de Jong D, Rubboli G, Talvik I, Sander V, Uldall P, Jacquemont ML, Nava C, Leguern E, Julia S, Gambardella A, d'Orsi G, Crichiutti G, Faivre L, Darmency V, Benova B, Krsek P, Biraben A, Lebre AS, Jennesson M, Sattar S, Marchal C, Nordli DR Jr, Lindstrom K, Striano P, Lomax LB, Kiss C, Bartolomei F, Lepine AF, Schoonjans AS, Stouffs K, Jansen A, Panagiotakaki E, Ricard-Mousnier B, Thevenon J, de Bellescize J, Catenoix

H, Dorn T, Zenker M, Müller-Schlüter K, Brandt C, Krey I, Polster T, Wolff M, Balci M, Rostasy K, Achaz G, Zacher P, Becher T, Cloppenborg T, Yuskaitis CJ, Weckhuysen S, Poduri A, Lemke JR, Møller RS, Baulac S. The landscape of epilepsy-related GATOR1 variants. Genet Med. 2019a Feb;21(2):398-408. doi: 10.1038/s41436-018-0060-2.

Baldassari S, Ribierre T, Marsan E, Adle-Biassette H, Ferrand-Sorbets S, Bulteau C, Dorison N, Fohlen M, Polivka M, Weckhuysen S, Dorfmüller G, Chipaux M, Baulac S. Dissecting the genetic basis of focal cortical dysplasia: a large cohort study. Acta Neuropathol. 2019b Aug 23. doi: 10.1007/s00401-019-02061-5.

Baldelli P, Fassio A, Valtorta F, Benfenati F. Lack of synapsin I reduces the readily releasable pool of synaptic vesicles at central inhibitory synapses. J Neurosci. 2007 Dec 5;27(49):13520-31. doi: 10.1523/JNEUROSCI.3151-07.2007.

Bar-Peled L, Chantranupong L, Cherniack AD, Chen WW, Ottina KA, Grabiner BC, Spear ED, Carter SL, Meyerson M, Sabatini DM. A Tumor suppressor complex with GAP activity for the Rag GTPases that signal amino acid sufficiency to mTORC1. Science. 2013 May 31;340(6136):1100-6. doi: 10.1126/science.1232044.

Bar-Peled L, Sabatini DM. Regulation of mTORC1 by amino acids. Trends Cell Biol. 2014 Jul;24(7):400-6. doi: 10.1016/j.tcb.2014.03.003.

Bateup HS, Denefrio CL, Johnson CA, Saulnier JL, Sabatini BL. Temporal dynamics of a homeostatic pathway controlling neural network activity. Front Mol Neurosci. 2013a Sep 18;6:28. doi: 10.3389/fnmol.2013.00028.

Bateup HS, Johnson CA, Denefrio CL, Saulnier JL, Kornacker K, Sabatini BL. Excitatory/inhibitory synaptic imbalance leads to hippocampal hyperexcitability in mouse models of tuberous sclerosis. Neuron. 2013b May 8;78(3):510-22. doi: 10.1016/j.neuron.2013.03.017.

Bateup HS, Takasaki KT, Saulnier JL, Denefrio CL, Sabatini BL. Loss of Tsc1 in vivo impairs hippocampal mGluR-LTD and increases excitatory synaptic function. J hhNeurosci. 2011 Jun 15;31(24):8862-9. doi: 10.1523/JNEUROSCI.1617-11.2011.

Baulac S, Ishida S, Marsan E, Miquel C, Biraben A, Nguyen DK, Nordli D, Cossette P, Nguyen S, Lambrecq V, Vlaicu M, Daniau M, Bielle F, Andermann E, Andermann F, Leguern E, Chassoux F, Picard F. Familial focal epilepsy with focal cortical

dysplasia due to DEPDC5 mutations. Ann Neurol. 2015 Apr;77(4):675-83. doi: 10.1002/ana.24368.

Baulac S, Ishida S, Marsan E, Miquel C, Biraben A, Nguyen DK, Nordli D, Cossette P, Nguyen S, Lambrecq V, Vlaicu M, Daniau M, Bielle F, Andermann E, Andermann F, Leguern E, Chassoux F, Picard F. Familial focal epilepsy with focal cortical dysplasia due to DEPDC5 mutations. Ann Neurol. 2015 Apr;77(4):675-83. doi: 10.1002/ana.24368.

Baulac S. mTOR signaling pathway genes in focal epilepsies. Prog Brain Res. 2016;226:61-79. doi: 10.1016/bs.pbr.2016.04.013.

Berkovic SF, Serratosa JM, Phillips HA, Xiong L, Andermann E, Díaz-Otero F, Gómez-Garre P, Martín M, Fernández-Bullido Y, Andermann F, Lopes-Cendes I, Dubeau F, Desbiens R, Scheffer IE, Wallace RH, Mulley JC, Pandolfo M. Familial partial epilepsy with variable foci: clinical features and linkage to chromosome 22q12. Epilepsia. 2004 Sep;45(9):1054-60.

Blümcke I, Thom M, Aronica E, Armstrong DD, Vinters HV, Palmini A, Jacques TS, Avanzini G, Barkovich AJ, Battaglia G, Becker A, Cepeda C, Cendes F, Colombo N, Crino P, Cross JH, Delalande O, Dubeau F, Duncan J, Guerrini R, Kahane P, Mathern G, Najm I, Ozkara C, Raybaud C, Represa A, Roper SN, Salamon N, Schulze-Bonhage A, Tassi L, Vezzani A, Spreafico R. The clinicopathologic spectrum of focal cortical dysplasias: a consensus classification proposed by an ad hoc Task Force of the ILAE Diagnostic Methods Commission. Epilepsia. 2011 Jan;52(1):158-74. doi: 10.1111/j.1528-1167.2010.02777.x.

Bockaert J, Marin P. mTOR in Brain Physiology and Pathologies. Physiol Rev. 2015 Oct;95(4):1157-87. doi: 10.1152/physrev.00038.2014.

Boonyapisit K, Najm I, Klem G, Ying Z, Burrier C, LaPresto E, Nair D, Bingaman W, Prayson R, Lüders H. Epileptogenicity of focal malformations due to abnormal cortical development: direct electrocorticographic-histopathologic correlations. Epilepsia. 2003 Jan;44(1):69-76.

Bozzi Y, Provenzano G, Casarosa S. Neurobiological bases of autism-epilepsy comorbidity: a focus on excitation/inhibition imbalance. Eur J Neurosci. 2018 Mar;47(6):534-548. doi: 10.1111/ejn.13595.

Brown EJ, Albers MW, Shin TB, Ichikawa K, Keith CT, Lane WS, Schreiber SL. A mammalian protein targeted by G1-arresting rapamycin-receptor complex. Nature. 1994 Jun 30;369(6483):756-8.

Browning RA, Nelson DK. Modification of electroshock and pentylenetetrazol seizure patterns in rats after precollicular transections. Exp Neurol. 1986 Sep;93(3):546-56.

Cafferkey R, Young PR, McLaughlin MM, Bergsma DJ, Koltin Y, Sathe GM, Faucette L, Eng WK, Johnson RK, Livi GP. Dominant missense mutations in a novel yeast protein related to mammalian phosphatidylinositol 3-kinase and VPS34 abrogate rapamycin cytotoxicity. Mol Cell Biol. 1993 Oct;13(10):6012-23.

Cammalleri M, Lütjens R, Berton F, King AR, Simpson C, Francesconi W, Sanna PP. Time-restricted role for dendritic activation of the mTOR-p70S6K pathway in the induction of late-phase long-term potentiation in the CA1. Proc Natl Acad Sci U S A. 2003 Nov 25;100(24):14368-73.

Cepeda C, André VM, Flores-Hernández J, Nguyen OK, Wu N, Klapstein GJ, Nguyen S, Koh S, Vinters HV, Levine MS, Mathern GW. Pediatric cortical dysplasia: correlations between neuroimaging, electrophysiology and location of cytomegalic neurons and balloon cells and glutamate/GABA synaptic circuits. Dev Neurosci. 2005 Jan-Feb;27(1):59-76.

Cepeda C, André VM, Hauptman JS, Yamazaki I, Huynh MN, Chang JW, Chen JY, Fisher RS, Vinters HV, Levine MS, Mathern GW. Enhanced GABAergic network and receptor function in pediatric cortical dysplasia Type IIB compared with Tuberous Sclerosis Complex. Neurobiol Dis. 2012 Jan;45(1):310-21. doi: 10.1016/j.nbd.2011.08.015.

Cepeda C, Chen JY, Wu JY, Fisher RS, Vinters HV, Mathern GW, Levine MS. Pacemaker GABA synaptic activity may contribute to network synchronization in pediatric cortical dysplasia. Neurobiol Dis. 2014 Feb;62:208-17. doi: 10.1016/j.nbd.2013.10.001. Epub 2013 Oct 10.

Cepeda C, Hurst RS, Flores-Hernández J, Hernández-Echeagaray E, Klapstein GJ, Boylan MK, Calvert CR, Jocoy EL, Nguyen OK, André VM, Vinters HV, Ariano MA, Levine MS, Mathern GW. Morphological and electrophysiological characterization of

abnormal cell types in pediatric cortical dysplasia. J Neurosci Res. 2003 May 15;72(4):472-86.

Chen J, Zheng XF, Brown EJ, Schreiber SL. Identification of an 11-kDa FKBP12-rapamycin-binding domain within the 289-kDa FKBP12-rapamycin-associated protein and characterization of a critical serine residue. Proc Natl Acad Sci USA. 1995 May 23;92(11):4947-51.

Chiappalone M, Casagrande S, Tedesco M, Valtorta F, Baldelli P, Martinoia S, Benfenati F. Opposite changes in glutamatergic and GABAergic transmission underlie the diffuse hyperexcitability of synapsin I-deficient cortical networks. Cereb Cortex. 2009 Jun;19(6):1422-39. doi: 10.1093/cercor/bhn182

Crino PB, Duhaime AC, Baltuch G, White R. Differential expression of glutamate and GABA-A receptor subunit mRNA in cortical dysplasia. Neurology. 2001 Apr 10;56(7):906-13.

Crino PB, Nathanson KL, Henske EP. The tuberous sclerosis complex. N Engl J Med. 2006 Sep 28;355(13):1345-56. Review.

Crino PB. Focal Cortical Dysplasia. Semin Neurol. 2015 Jun;35(3):201-8. doi: 10.1055/s-0035-1552617. Epub 2015 Jun 10. Review.

Cunningham JT, Rodgers JT, Arlow DH, Vazquez F, Mootha VK, Puigserver P. mTOR controls mitochondrial oxidative function through a YY1-PGC-1alpha transcriptional complex. Nature. 2007 Nov 29;450(7170):736-40.

de Calbiac H, Dabacan A, Marsan E, Tostivint H, Devienne G, Ishida S, Leguern E, Baulac S, Muresan RC, Kabashi E, Ciura S. Depdc5 knockdown causes mTOR-dependent motor hyperactivity in zebrafish. Ann Clin Transl Neurol. 2018 Apr 6;5(5):510-523. doi: 10.1002/acn3.542

D'Gama AM, Woodworth MB, Hossain AA, Bizzotto S, Hatem NE, LaCoursiere CM, Najm I, Ying Z, Yang E, Barkovich AJ, Kwiatkowski DJ, Vinters HV, Madsen JR, Mathern GW, Blümcke I, Poduri A, Walsh CA. Somatic Mutations Activating the mTOR Pathway in Dorsal Telencephalic Progenitors Cause a Continuum of Cortical Dysplasias. Cell Rep. 2017 Dec 26;21(13):3754-3766. doi: 10.1016/j.celrep.2017.11.106.

Dibbens LM, de Vries B, Donatello S, Heron SE, Hodgson BL, Chintawar S, Crompton DE, Hughes JN, Bellows ST, Klein KM, Callenbach PM, Corbett MA, Gardner AE, Kivity S, Iona X, Regan BM, Weller CM, Crimmins D, O'Brien TJ, Guerrero-López R, Mulley JC, Dubeau F, Licchetta L, Bisulli F, Cossette P, Thomas PQ, Gecz J, Serratosa J, Brouwer OF, Andermann F, Andermann E, van den Maagdenberg AM, Pandolfo M, Berkovic SF, Scheffer IE. Mutations in DEPDC5 cause familial focal epilepsy with variable foci. Nat Genet. 2013 May;45(5):546-51. doi: 10.1038/ng.2599.

Dibble CC, Elis W, Menon S, Qin W, Klekota J, Asara JM, Finan PM, Kwiatkowski DJ, Murphy LO, Manning BD. TBC1D7 is a third subunit of the TSC1-TSC2 complex upstream of mTORC1. Mol Cell. 2012 Aug 24;47(4):535-46. doi: 10.1016/j.molcel.2012.06.009.

Ehninger D. From genes to cognition in tuberous sclerosis: implications for mTOR inhibitor-based treatment approaches. Neuropharmacology. 2013 May;68:97-105. doi: 10.1016/j.neuropharm.2012.05.015.

Endersby R, Baker SJ. PTEN signaling in brain: neuropathology and tumorigenesis. Oncogene. 2008 Sep 18;27(41):5416-30. doi: 10.1038/onc.2008.239. Review.

Fassio A, Esposito A, Kato M, Saitsu H, Mei D, Marini C, Conti V, Nakashima M, Okamoto N, Olmez Turker A, Albuz B, Semerci Gündüz CN, Yanagihara K, Belmonte E, Maragliano L, Ramsey K, Balak C, Siniard A, Narayanan V; C4RCD Research Group, Ohba C, Shiina M, Ogata K, Matsumoto N, Benfenati F, Guerrini R. De novo mutations of the ATP6V1A gene cause developmental encephalopathy with epilepsy. Brain. 2018 Jun 1;141(6):1703-1718. doi: 10.1093/brain/awy092.

Fauser S, Häussler U, Donkels C, Huber S, Nakagawa J, Prinz M, Schulze-Bonhage A, Zentner J, Haas CA. Disorganization of neocortical lamination in focal cortical dysplasia is brain-region dependent: evidence from layer-specific marker expression. Acta Neuropathol Commun. 2013 Aug 8;1:47. doi: 10.1186/2051-5960-1-47.

Fraser MM, Zhu X, Kwon CH, Uhlmann EJ, Gutmann DH, Baker SJ. Pten loss causes hypertrophy and increased proliferation of astrocytes in vivo. Cancer Res. 2004 Nov 1;64(21):7773-9.

Glick D, Barth S, Macleod KF. Autophagy: cellular and molecular mechanisms. J Pathol. 2010 May;221(1):3-12. doi: 10.1002/path.2697.

Gregorian C, Nakashima J, Le Belle J, Ohab J, Kim R, Liu A, Smith KB, Groszer M, Garcia AD, Sofroniew MV, Carmichael ST, Kornblum HI, Liu X, Wu H. Pten deletion in adult neural stem/progenitor cells enhances constitutive neurogenesis. J Neurosci. 2009 Feb 11;29(6):1874-86. doi: 10.1523/JNEUROSCI.3095-08.2009.

Guertin DA, Stevens DM, Thoreen CC, Burds AA, Kalaany NY, Moffat J, Brown M, Fitzgerald KJ, Sabatini DM. Ablation in mice of the mTORC components raptor, rictor, or mLST8 reveals that mTORC2 is required for signaling to Akt-FOXO and PKCalpha, but not S6K1. Dev Cell. 2006 Dec;11(6):859-71.

Hall MN. mTOR-what does it do? Transplant Proc. 2008 Dec;40(10 Suppl):S5-8. doi: 10.1016/j.transproceed.2008.10.009.

Hay N, Sonenberg N. Upstream and downstream of mTOR. Genes Dev. 2004 Aug 15;18(16):1926-45. Review.

Helliwell SB, Wagner P, Kunz J, Deuter-Reinhard M, Henriquez R, Hall MN. TOR1 and TOR2 are structurally and functionally similar but not identical phosphatidylinositol kinase homologues in yeast. Mol Biol Cell. 1994 Jan;5(1):105-18.

Hentges KE, Sirry B, Gingeras AC, Sarbassov D, Sonenberg N, Sabatini D, Peterson AS. FRAP/mTOR is required for proliferation and patterning during embryonic development in the mouse. Proc Natl Acad Sci U S A. 2001 Nov 20;98(24):13796-801.

Heron SE, Smith KR, Bahlo M, Nobili L, Kahana E, Licchetta L, Oliver KL, Mazarib A, Afawi Z, Korczyn A, Plazzi G, Petrou S, Berkovic SF, Scheffer IE, Dibbens LM. Missense mutations in the sodium-gated potassium channel gene KCNT1 cause severe autosomal dominant nocturnal frontal lobe epilepsy. Nat Genet. 2012 Nov;44(11):1188-90. doi: 10.1038/ng.2440.

Hilbig A, Babb TL, Najm I, Ying Z, Wyllie E, Bingaman W. Focal cortical dysplasia in children. Dev Neurosci. 1999 Nov;21(3-5):271-80.

Hoeffer CA, Klann E. mTOR signaling: at the crossroads of plasticity, memory and disease. Trends Neurosci. 2010 Feb;33(2):67-75. doi: 10.1016/j.tins.2009.11.003.

Hosokawa N, Hara T, Kaizuka T, Kishi C, Takamura A, Miura Y, Iemura S, Natsume T, Takehana K, Yamada N, Guan JL, Oshiro N, Mizushima N. Nutrient-dependent mTORC1 association with the ULK1-Atg13-FIP200 complex required for autophagy. Mol Biol Cell. 2009 Apr;20(7):1981-91. doi: 10.1091/mbc.E08-12-1248.

Howell JJ, Manning BD. mTOR couples cellular nutrient sensing to organismal metabolic homeostasis. Trends Endocrinol Metab. 2011 Mar;22(3):94-102. doi: 10.1016/j.tem.2010.12.003.

Hu S, Knowlton RC, Watson BO, Glanowska KM, Murphy GG, Parent JM, Wang Y. Somatic Depdc5 deletion recapitulates electroclinical features of human focal cortical dysplasia type IIA. Ann Neurol. 2018 Jul;84(1):140-146. doi: 10.1002/ana.25272.

Hughes J, Dawson R, Tea M, McAninch D, Piltz S, Jackson D, Stewart L, Ricos MG, Dibbens LM, Harvey NL, Thomas P. Knockout of the epilepsy gene Depdc5 in mice causes severe embryonic dysmorphology with hyperactivity of mTORC1 signalling. Sci Rep. 2017 Oct 3;7(1):12618. doi: 10.1038/s41598-017-12574-2.

Iadevaia V, Liu R, Proud CG. mTORC1 signaling controls multiple steps in ribosome biogenesis. Semin Cell Dev Biol. 2014 Dec;36:113-20. doi: 10.1016/j.semcdb.2014.08.004.

Iffland PH 2nd, Baybis M, Barnes AE, Leventer RJ, Lockhart PJ, Crino PB. DEPDC5 and NPRL3 modulate cell size, filopodial outgrowth, and localization of mTOR in neural progenitor cells and neurons. Neurobiol Dis. 2018 Jun;114:184-193. doi: 10.1016/j.nbd.2018.02.013.

Iffland PH 2nd, Crino PB. Focal Cortical Dysplasia: Gene Mutations, Cell Signaling, and Therapeutic Implications. Annu Rev Pathol. 2017 Jan 24;12:547-571. doi: 10.1146/annurev-pathol-052016-100138.

Inoki K, Li Y, Xu T, Guan KL. Rheb GTPase is a direct target of TSC2 GAP activity and regulates mTOR signaling. Genes Dev. 2003 Aug 1;17(15):1829-34.

Inoki K, Li Y, Zhu T, Wu J, Guan KL. TSC2 is phosphorylated and inhibited by Akt and suppresses mTOR signalling. Nat Cell Biol. 2002 Sep;4(9):648-57.

Ishida S, Picard F, Rudolf G, Noé E, Achaz G, Thomas P, Genton P, Mundwiller E, Wolff M, Marescaux C, Miles R, Baulac M, Hirsch E, Leguern E, Baulac S. Mutations of DEPDC5 cause autosomal dominant focal epilepsies. Nat Genet. 2013 May;45(5):552-5. doi: 10.1038/ng.2601.

Jaworski J, Spangler S, Seeburg DP, Hoogenraad CC, Sheng M. Control of dendritic arborization by the phosphoinositide-3'-kinase-Akt-mammalian target of rapamycin pathway. J Neurosci. 2005 Dec 7;25(49):11300-12.

Jung CH, Jun CB, Ro SH, Kim YM, Otto NM, Cao J, Kundu M, Kim DH. ULK-Atg13-FIP200 complexes mediate mTOR signaling to the autophagy machinery. Mol Biol Cell. 2009 Apr;20(7):1992-2003. doi: 10.1091/mbc.E08-12-1249.

Kim HJ, Cho MH, Shim WH, Kim JK, Jeon EY, Kim DH, Yoon SY. Deficient autophagy in microglia impairs synaptic pruning and causes social behavioral defects. Mol Psychiatry. 2017 Nov;22(11):1576-1584. doi: 10.1038/mp.2016.103.

Kim HW, Ha SH, Lee MN, Huston E, Kim DH, Jang SK, Suh PG, Houslay MD, Ryu SH. Cyclic AMP controls mTOR through regulation of the dynamic interaction between Rheb and phosphodiesterase 4D. Mol Cell Biol. 2010 Nov;30(22):5406-20. doi: 10.1128/MCB.00217-10.

Kim J, Kundu M, Viollet B, Guan KL. AMPK and mTOR regulate autophagy through direct phosphorylation of Ulk1. Nat Cell Biol. 2011 Feb;13(2):132-41. doi: 10.1038/ncb2152.

Kumar V, Zhang MX, Swank MW, Kunz J, Wu GY. Regulation of dendritic morphogenesis by Ras-PI3K-Akt-mTOR and Ras-MAPK signaling pathways. J Neurosci. 2005 Dec 7;25(49):11288-99.

Kunz J, Henriquez R, Schneider U, Deuter-Reinhard M, Movva NR, Hall MN. Target of rapamycin in yeast, TOR2, is an essential phosphatidylinositol kinase homolog required for G1 progression. Cell. 1993 May 7;73(3):585-96.

Laplante M, Sabatini DM. mTOR signaling in growth control and disease. Cell. 2012 Apr 13;149(2):274-93. doi: 10.1016/j.cell.2012.03.017. Review.

Lasarge CL, Danzer SC. Mechanisms regulating neuronal excitability and seizure development following mTOR pathway hyperactivation. Front Mol Neurosci. 2014 Mar 14;7:18. doi: 10.3389/fnmol.2014.00018.

Lee S, Kim SH, Kim B, Lee ST, Choi JR, Kim HD, Lee JS, Kang HC. Clinical Implementation of Targeted Gene Sequencing for Malformation of Cortical Development. Pediatr Neurol. 2019 Jul 26. pii: S0887-8994(19)30097-9. doi: 10.1016/j.pediatrneurol.2019.07.010.

Long X, Lin Y, Ortiz-Vega S, Yonezawa K, Avruch J. Rheb binds and regulates the mTOR kinase. Curr Biol. 2005 Apr 26;15(8):702-13.

Luikart BW, Schnell E, Washburn EK, Bensen AL, Tovar KR, Westbrook GL. Pten knockdown in vivo increases excitatory drive onto dentate granule cells. J Neurosci. 2011 Mar 16;31(11):4345-54. doi: 10.1523/JNEUROSCI.0061-11.2011.

Malagelada C, López-Toledano MA, Willett RT, Jin ZH, Shelanski ML, Greene LA. RTP801/REDD1 regulates the timing of cortical neurogenesis and neuron migration. J Neurosci. 2011 Mar 2;31(9):3186-96. doi: 10.1523/JNEUROSCI.4011-10.2011.

Marsan E, Baulac S. Mechanistic target of rapamycin (mTOR) pathway, focal cortical dysplasia and epilepsy. Neuropathol Appl Neurobiol. 2018 Feb;44(1):6-17. doi: 10.1111/nan.12463.

Marsan E, Ishida S, Schramm A, Weckhuysen S, Muraca G, Lecas S, Liang N, Treins C, Pende M, Roussel D, Le Van Quyen M, Mashimo T, Kaneko T, Yamamoto T, Sakuma T, Mahon S, Miles R, Leguern E, Charpier S, Baulac S. Depdc5 knockout rat: A novel model of mTORopathy. Neurobiol Dis. 2016 May;89:180-9. doi: 10.1016/j.nbd.2016.02.010.

Martin C, Meloche C, Rioux MF, Nguyen DK, Carmant L, Andermann E, Gravel M, Cossette P. A recurrent mutation in DEPDC5 predisposes to focal epilepsies in the French-Canadian population. Clin Genet. 2014 Dec;86(6):570-4. doi: 10.1111/cge.12311.

McMahon J, Huang X, Yang J, Komatsu M, Yue Z, Qian J, Zhu X, Huang Y. Impaired autophagy in neurons after disinhibition of mammalian target of rapamycin and its contribution to epileptogenesis. J Neurosci. 2012 Nov 7;32(45):15704-14. doi: 10.1523/JNEUROSCI.2392-12.2012.

Meikle L, Pollizzi K, Egnor A, Kramvis I, Lane H, Sahin M, Kwiatkowski DJ. Response of a neuronal model of tuberous sclerosis to mammalian target of rapamycin (mTOR) inhibitors: effects on mTORC1 and Akt signaling lead to improved survival and function. J Neurosci. 2008 May 21;28(21):5422-32. doi: 10.1523/JNEUROSCI.0955-08.2008.

Miyahara H, Natsumeda M, Shiga A, Aoki H, Toyoshima Y, Zheng Y, Takeuchi R, Murakami H, Masuda H, Kameyama S, Izumi T, Fujii Y, Takahashi H, Kakita A. Suppressed expression of autophagosomal protein LC3 in cortical tubers of tuberous

sclerosis complex. Brain Pathol. 2013 May;23(3):254-62. doi: 10.1111/j.1750-3639.2012.00634.x.

Murakami M, Ichisaka T, Maeda M, Oshiro N, Hara K, Edenhofer F, Kiyama H, Yonezawa K, Yamanaka S. mTOR is essential for growth and proliferation in early mouse embryos and embryonic stem cells. Mol Cell Biol. 2004 Aug;24(15):6710-8.

Orlova KA, Tsai V, Baybis M, Heuer GG, Sisodiya S, Thom M, Strauss K, Aronica E, Storm PB, Crino PB. Early progenitor cell marker expression distinguishes type II from type I focal cortical dysplasias. J Neuropathol Exp Neurol. 2010 Aug;69(8):850-63. doi: 10.1097/NEN.0b013e3181eac1f5.

Osborne LR. Caveat mTOR: aberrant signaling disrupts corticogenesis. J Clin Invest. 2010 May;120(5):1392-5. doi: 10.1172/JCI43030.

Ottman R, Winawer MR, Kalachikov S, Barker-Cummings C, Gilliam TC, Pedley TA, Hauser WA. LGI1 mutations in autosomal dominant partial epilepsy with auditory features. Neurology. 2004 Apr 13;62(7):1120-6.

Padi SKR, Singh N, Bearss JJ, Olive V, Song JH, Cardó-Vila M, Kraft AS, Okumura K. Phosphorylation of DEPDC5, a component of the GATOR1 complex, releases inhibition of mTORC1 and promotes tumor growth. Proc Natl Acad Sci U S A. 2019 Sep 23. pii: 201904774. doi: 10.1073/pnas.1904774116.

Panchaud N, Péli-Gulli MP, De Virgilio C. Amino acid deprivation inhibits TORC1 through a GTPase-activating protein complex for the Rag family GTPase Gtr1. Sci Signal. 2013 May 28;6(277):ra42. doi: 10.1126/scisignal.2004112.

Panja D, Dagyte G, Bidinosti M, Wibrand K, Kristiansen AM, Sonenberg N, Bramham CR. Novel translational control in Arc-dependent long term potentiation consolidation in vivo. J Biol Chem. 2009 Nov 13;284(46):31498-511. doi: 10.1074/jbc.M109.056077.

Park SM, Lim JS, Ramakrishina S, Kim SH, Kim WK, Lee J, Kang HC, Reiter JF, Kim DS, Kim HH, Lee JH. Brain somatic mutations in mTOR disrupt neuronal ciliogenesis, leading to focal cortical dyslamination. Neuron. 2018 Jul 11;99(1):83-97.e7. doi: 10.1016/j.neuron.2018.05.039.

Patterson SL, Pittenger C, Morozov A, Martin KC, Scanlin H, Drake C, Kandel ER. Some forms of cAMP-mediated long-lasting potentiation are associated with release of

BDNF and nuclear translocation of phospho-MAP kinase. Neuron. 2001 Oct 11;32(1):123-40.

Peña-Llopis S, Vega-Rubin-de-Celis S, Schwartz JC, Wolff NC, Tran TA, Zou L, Xie XJ, Corey DR, Brugarolas J. Regulation of TFEB and V-ATPases by mTORC1. EMBO J. 2011 Jul 29;30(16):3242-58. doi: 10.1038/emboj.2011.257.

Picard F, Makrythanasis P, Navarro V, Ishida S, de Bellescize J, Ville D, Weckhuysen S, Fosselle E, Suls A, De Jonghe P, Vasselon Raina M, Lesca G, Depienne C, An-Gourfinkel I, Vlaicu M, Baulac M, Mundwiller E, Couarch P, Combi R, Ferini-Strambi L, Gambardella A, Antonarakis SE, Leguern E, Steinlein O, Baulac S. DEPDC5 mutations in families presenting as autosomal dominant nocturnal frontal lobe epilepsy. Neurology. 2014 Jun 10;82(23):2101-6. doi: 10.1212/WNL.0000000000000488.

Poduri A. DEPDC5 does it all: shared genetics for diverse epilepsy syndromes. Ann Neurol. 2014 May;75(5):631-3. doi: 10.1002/ana.24160.

Porstmann T, Santos CR, Griffiths B, Cully M, Wu M, Leevers S, Griffiths JR, Chung YL, Schulze A. SREBP activity is regulated by mTORC1 and contributes to Akt-dependent cell growth. Cell Metab. 2008 Sep;8(3):224-36. doi: 10.1016/j.cmet.2008.07.007.

Prestigio C, Ferrante D, Valente P, Casagrande S, Albanesi E, Yanagawa Y, Benfenati F, Baldelli P. Spike-Related Electrophysiological Identification of Cultured Hippocampal Excitatory and Inhibitory Neurons. Mol Neurobiol. 2019 Feb 12. doi: 10.1007/s12035-019-1506-5.

Raab-Graham KF, Haddick PC, Jan YN, Jan LY. Activity- and mTOR-dependent suppression of Kv1.1 channel mRNA translation in dendrites. Science. 2006 Oct 6;314(5796):144-8.

Ran I, Gkogkas CG, Vasuta C, Tartas M, Khoutorsky A, Laplante I, Parsyan A, Nevarko T, Sonenberg N, Lacaille JC. Selective regulation of GluA subunit synthesis and AMPA receptor-mediated synaptic function and plasticity by the translation repressor 4E-BP2 in hippocampal pyramidal cells. J Neurosci. 2013 Jan 30;33(5):1872-86. doi: 10.1523/JNEUROSCI.3264-12.2013.

Ribierre T, Deleuze C, Bacq A, Baldassari S, Marsan E, Chipaux M, Muraca G, Roussel D, Navarro V, Leguern E, Miles R, Baulac S. Second-hit mosaic mutation in

mTORC1 repressor DEPDC5 causes focal cortical dysplasia-associated epilepsy. J Clin Invest. 2018 Jun 1;128(6):2452-2458. doi: 10.1172/JCI99384.

Sabatini DM, Erdjument-Bromage H, Lui M, Tempst P, Snyder SH. RAFT1: a mammalian protein that binds to FKBP12 in a rapamycin-dependent fashion and is homologous to yeast TORs. Cell. 1994 Jul 15;78(1):35-43.

Sabers CJ, Martin MM, Brunn GJ, Williams JM, Dumont FJ, Wiederrecht G, Abraham RT. Isolation of a protein target of the FKBP12-rapamycin complex in mammalian cells. J Biol Chem. 1995 Jan 13;270(2):815-22.

Salamon N, Andres M, Chute DJ, Nguyen ST, Chang JW, Huynh MN, Chandra PS, Andre VM, Cepeda C, Levine MS, Leite JP, Neder L, Vinters HV, Mathern GW. Contralateral hemimicrencephaly and clinical-pathological correlations in children with hemimegalencephaly. Brain. 2006 Feb;129(Pt 2):352-65.

Sancak Y, Bar-Peled L, Zoncu R, Markhard AL, Nada S, Sabatini DM. Ragulator-Rag complex targets mTORC1 to the lysosomal surface and is necessary for its activation by amino acids. Cell. 2010 Apr 16;141(2):290-303. doi: 10.1016/j.cell.2010.02.024.

Sancak Y, Peterson TR, Shaul YD, Lindquist RA, Thoreen CC, Bar-Peled L, Sabatini DM. The Rag GTPases bind raptor and mediate amino acid signaling to mTORC1. Science. 2008 Jun 13;320(5882):1496-501. doi: 10.1126/science.1157535.

Sangüesa G, Roglans N, Baena M, Velázquez AM, Laguna JC, Alegret M. mTOR is a Key Protein Involved in the Metabolic Effects of Simple Sugars. Int J Mol Sci. 2019 Mar 5;20(5). pii: E1117. doi: 10.3390/ijms20051117.

Scheffer IE, Heron SE, Regan BM, Mandelstam S, Crompton DE, Hodgson BL, Licchetta L, Provini F, Bisulli F, Vadlamudi L, Gecz J, Connelly A, Tinuper P, Ricos MG, Berkovic SF, Dibbens LM. Mutations in mammalian target of rapamycin regulator DEPDC5 cause focal epilepsy with brain malformations. Ann Neurol. 2014 May;75(5):782-7. doi: 10.1002/ana.24126.

Sekiguchi T, Hirose E, Nakashima N, Ii M, Nishimoto T. Novel G proteins, Rag C and Rag D, interact with GTP-binding proteins, Rag A and Rag B. J Biol Chem. 2001 Mar 9;276(10):7246-57.

Shehata M, Matsumura H, Okubo-Suzuki R, Ohkawa N, Inokuchi K. Neuronal stimulation induces autophagy in hippocampal neurons that is involved in AMPA

receptor degradation after chemical long-term depression. J Neurosci. 2012 Jul 25;32(30):10413-22. doi: 10.1523/JNEUROSCI.4533-11.2012.

Shiota C, Woo JT, Lindner J, Shelton KD, Magnuson MA. Multiallelic disruption of the rictor gene in mice reveals that mTOR complex 2 is essential for fetal growth and viability. Dev Cell. 2006 Oct;11(4):583-9.

Sim NS, Ko A, Kim WK, Kim SH, Kim JS, Shim KW, Aronica E, Mijnsbergen C, Spliet WGM, Koh HY, Kim HD, Lee JS, Kim DS, Kang HC, Lee JH. Precise detection of low-level somatic mutation in resected epilepsy brain tissue. Acta Neuropathol. 2019 Dec;138(6):901-912. doi: 10.1007/s00401-019-02052-6.

Skarnes WC, Rosen B, West AP, Koutsourakis M, Bushell W, Iyer V, Mujica AO, Thomas M, Harrow J, Cox T, Jackson D, Severin J, Biggs P, Fu J, Nefedov M, de Jong PJ, Stewart AF, Bradley A. A conditional knockout resource for the genome-wide study of mouse gene function. Nature. 2011 Jun 15;474(7351):337-42. doi: 10.1038/nature10163.

Stafstrom CE. Recognizing Seizures and Epilepsy: Insights from Pathophysiology. In Epilepsy. Wiley Blackwell. 2014. p. 1-9. doi: 10.1002/9781118456989.ch1.

Stewart SA, Dykxhoorn DM, Palliser D, Mizuno H, Yu EY, An DS, Sabatini DM, Chen IS, Hahn WC, Sharp PA, Weinberg RA, Novina CD. Lentivirus-delivered stable gene silencing by RNAi in primary cells. RNA. 2003 Apr;9(4):493-501. doi: 10.1261/rna.2192803.

Swaminathan A, Hassan-Abdi R, Renault S, Siekierska A, Riché R, Liao M, de Witte PAM, Yanicostas C, Soussi-Yanicostas N, Drapeau P, Samarut É. Non-canonical mTOR-Independent-Role of DEPDC5 in Regulating GABAergic Network Development. Curr Biol. 2018 Jun 18;28(12):1924-1937.e5. doi: 10.1016/j.cub.2018.04.061.

Talos DM, Kwiatkowski DJ, Cordero K, Black PM, Jensen FE. Cell-specific alterations of glutamate receptor expression in tuberous sclerosis complex cortical tubers. Ann Neurol. 2008 Apr;63(4):454-65. doi: 10.1002/ana.21342.

Tang G, Gudsnuk K, Kuo SH, Cotrina ML, Rosoklija G, Sosunov A, Sonders MS, Kanter E, Castagna C, Yamamoto A, Yue Z, Arancio O, Peterson BS, Champagne F, Dwork AJ, Goldman J, Sulzer D. Loss of mTOR-dependent macroautophagy causes

autistic-like synaptic pruning deficits. Neuron. 2014 Sep 3;83(5):1131-43. doi: 10.1016/j.neuron.2014.07.040.

Tang SJ, Reis G, Kang H, Gingras AC, Sonenberg N, Schuman EM. A rapamycin-sensitive signaling pathway contributes to long-term synaptic plasticity in the hippocampus. Proc Natl Acad Sci U S A. 2002 Jan 8;99(1):467-72.

Tassi L, Colombo N, Garbelli R, Francione S, Lo Russo G, Mai R, Cardinale F, Cossu M, Ferrario A, Galli C, Bramerio M, Citterio A, Spreafico R. Focal cortical dysplasia: neuropathological subtypes, EEG, neuroimaging and surgical outcome. Brain. 2002 Aug;125(Pt 8):1719-32.

Tavazoie SF, Alvarez VA, Ridenour DA, Kwiatkowski DJ, Sabatini BL. Regulation of neuronal morphology and function by the tumor suppressors Tsc1 and Tsc2. Nat Neurosci. 2005 Dec;8(12):1727-34.

Tsai PT, Hull C, Chu Y, Greene-Colozzi E, Sadowski AR, Leech JM, Steinberg J, Crawley JN, Regehr WG, Sahin M. Autistic-like behaviour and cerebellar dysfunction in Purkinje cell Tsc1 mutant mice. Nature. 2012 Aug 30;488(7413):647-51. doi: 10.1038/nature11310.

Valente P, Lignani G, Medrihan L, Bosco F, Contestabile A, Lippiello P, Ferrea E, Schachner M, Benfenati F, Giovedì S, Baldelli P. Cell adhesion molecule L1 contributes to neuronal excitability regulating the function of voltage-gated Na+ channels. J Cell Sci. 2016 May 1;129(9):1878-91. doi: 10.1242/jcs.182089.

Wang Y, Barbaro MF, Baraban SC. A role for the mTOR pathway in surface expression of AMPA receptors. Neurosci Lett. 2006 Jun 19;401(1-2):35-9.

White R, Hua Y, Scheithauer B, Lynch DR, Henske EP, Crino PB. Selective alterations in glutamate and GABA receptor subunit mRNA expression in dysplastic neurons and giant cells of cortical tubers. Ann Neurol. 2001 Jan;49(1):67-78.

Wong M. A critical review of mTOR inhibitors and epilepsy: from basic science to clinical trials. Expert Rev Neurother. 2013 Jun;13(6):657-69. doi: 10.1586/ern.13.48. Review.

Wu R, Wu H. A molecular chaperone mediates a two-protein enzyme complex and glycosylation of serine-rich streptococcal adhesins. J Biol Chem. 2011 Oct 7;286(40):34923-31. doi: 10.1074/jbc.M111.239350.

Yasin SA, Ali AM, Tata M, Picker SR, Anderson GW, Latimer-Bowman E, Nicholson SL, Harkness W, Cross JH, Paine SM, Jacques TS. mTOR-dependent abnormalities in autophagy characterize human malformations of cortical development: evidence from focal cortical dysplasia and tuberous sclerosis. Acta Neuropathol. 2013 Aug;126(2):207-18. doi: 10.1007/s00401-013-1135-4.

Yu L, McPhee CK, Zheng L, Mardones GA, Rong Y, Peng J, Mi N, Zhao Y, Liu Z, Wan F, Hailey DW, Oorschot V, Klumperman J, Baehrecke EH, Lenardo MJ. Termination of autophagy and reformation of lysosomes regulated by mTOR. Nature. 2010 Jun 17;465(7300):942-6. doi: 10.1038/nature09076.

Yuskaitis CJ, Jones BM, Wolfson RL, Super CE, Dhamne SC, Rotenberg A, Sabatini DM, Sahin M, Poduri A. A mouse model of DEPDC5-related epilepsy: Neuronal loss of Depdc5 causes dysplastic and ectopic neurons, increased mTOR signaling, and seizure susceptibility. Neurobiol Dis. 2018 Mar;111:91-101. doi: 10.1016/j.nbd.2017.12.010.

Zeng M, Zhou JN. Roles of autophagy and mTOR signaling in neuronal differentiation of mouse neuroblastoma cells. Cell Signal. 2008 Apr;20(4):659-65. doi: 10.1016/j.cellsig.2007.11.015.

Zhang Y, Nicholatos J, Dreier JR, Ricoult SJ, Widenmaier SB, Hotamisligil GS, Kwiatkowski DJ, Manning BD. Coordinated regulation of protein synthesis and degradation by mTORC1. Nature. 2014 Sep 18;513(7518):440-3. doi: 10.1038/nature13492.

Zoncu R, Bar-Peled L, Efeyan A, Wang S, Sancak Y, Sabatini DM. mTORC1 senses lysosomal amino acids through an inside-out mechanism that requires the vacuolar H(+)-ATPase. Science. 2011 Nov 4;334(6056):678-83. doi: 10.1126/science.1207056.

Zoncu R, Efeyan A, Sabatini DM. mTOR: from growth signal integration to cancer, diabetes and ageing. Nat Rev Mol Cell Biol. 2011 Jan;12(1):21-35. doi: 10.1038/nrm3025. Epub 2010 Dec 15. Review.

10. Appendix

Articles published/ in publication by Antonio De Fusco during the PhD course.

De Fusco A[#], Cerullo MS[#], Marte A, Michetti C, Romei A, Castroflorio E, Baulac S, Benfenati F. Acute knockdown of Depdc5 leads to synaptic defects in mTOR-related epileptogenesis. Under review.

#: Equal contribution

DEP-domain containing 5 (DEPDC5) is part of the GATOR1 complex that functions as key inhibitor of the mechanistic target of rapamycin complex 1 (mTORC1). Loss-of-function mutations in DEPDC5 leading to mTOR hyperactivation have been identified as the most common cause of either lesional or non-lesional focal epilepsy. However, the precise mechanisms by which DEPDC5 loss-of-function triggers neuronal and network hyperexcitability are still unclear. In this study, we investigated the cellular mechanisms of hyperexcitability by comparing the constitutive heterozygous Depdc5 knockout mouse versus different levels of acute Depdc5 deletion (≈40% and ≈80% neuronal knockdown of Depdc5 protein) by RNA interference in primary cortical cultures. While heterozygous Depdc5+/- neurons have only a subtle phenotype, acutely knocked-down neurons exhibit a strong dose-dependent phenotype characterized by mTOR hyperactivation, increased soma size, dendritic arborization, excitatory synaptic transmission and intrinsic excitability. The robust synaptic phenotype resulting from the acute knockdown Depdc5 deficiency highlights the importance of the temporal dynamics of Depdc5 knockdown in triggering the phenotypic changes, reminiscent of the somatic second-hit mechanism in patients with focal cortical dysplasia. These findings uncover a novel synaptic phenotype that is causally linked to Depdc5 knockdown, highlighting the developmental role of Depdc5. Interestingly, the synaptic defect appears to affect only excitatory synapses, while inhibitory synapses develop normally. The increased frequency and amplitude of mEPSCs, paralleled by increased density of excitatory synapses and expression of glutamate receptors, may generate an excitation/inhibition imbalance that triggers epileptogenesis.

Rocchi A, Sacchetti S, **De Fusco A**, Giovedi S, Parisi B, Cesca F, Höltje M, Ruprecht K, Ahnert-Hilger G, Benfenati F. Autoantibodies to synapsin I sequestrate synapsin I and alter synaptic function. Cell Death Dis. 2019 Nov 14;10(11):864. doi: 10.1038/s41419-019-2106-z.

Synapsin I is a phosphoprotein that coats the cytoplasmic side of synaptic vesicles and regulates their trafficking within nerve terminals. Autoantibodies against Syn I have been described in sera and cerebrospinal fluids of patients with numerous neurological diseases, including limbic encephalitis and clinically isolated syndrome; however, the effects and fate of autoantibodies in neurons are still unexplored. We found that in vitro exposure of primary hippocampal neurons to patient's autoantibodies to SynI decreased the density of excitatory and inhibitory synapses and impaired both glutamatergic and GABAergic synaptic transmission. These effects were reproduced with a purified SynI antibody and completely absent in SynI knockout neurons. Autoantibodies to SynI are internalized by FcγII/III-mediated endocytosis, interact with endogenous SynI, and promote its sequestration and intracellular aggregation. Neurons exposed to human autoantibodies to SynI display a reduced density of SVs, mimicking the SynI loss-of-function phenotype. Our data indicate that autoantibodies to intracellular antigens such as SynI can reach and inactivate their targets and suggest that an antibody-mediated synaptic dysfunction may contribute to the evolution and progression of autoimmune-mediated neurological diseases positive for SynI autoantibodies.

Esposito A, Falace A, Wagner M, Gal M, Mei D, Conti V, Pisano T, Aprile D, Cerullo MS, **De Fusco A**, Giovedì S, Seibt A, Magen D, Polster T, Eran A, Stenton SL, Fiorillo C, Ravid S, Mayatepek E, Hafner H, Wortmann S, Levanon EY, Marini C, Mandel H, Benfenati F, Distelmaier F, Fassio A, Guerrini R. Biallelic DMXL2 mutations impair autophagy and cause Ohtahara syndrome with progressive course. Brain. 2019 Dec 1;142(12):3876-3891. doi: 10.1093/brain/awz326.

Ohtahara syndrome, early infantile epileptic encephalopathy with a suppression burst EEG pattern, is an aetiologically heterogeneous condition starting in the first weeks or months of life with intractable seizures and profound developmental disability. Using whole exome sequencing, we identified biallelic DMXL2 mutations in three sibling pairs with Ohtahara syndrome, belonging to three unrelated families. Siblings in Family 1 were compound heterozygous for the c.5135C>T (p.Ala1712Val) missense substitution and the c.4478C>G (p.Ser1493*) nonsense substitution; in Family 2 were homozygous for the c.4478C>A (p.Ser1493*) nonsense substitution and in Family 3 were homozygous for the c.7518-1G>A (p.Trp2507Argfs*4) substitution. The severe developmental and epileptic encephalopathy manifested from the first day of life and was associated with deafness, mild peripheral polyneuropathy and dysmorphic features. Early brain MRI investigations in the first months of life revealed thin corpus callosum with brain hypomyelination in all. Follow-up MRI scans in three patients revealed progressive moderate brain shrinkage with leukoencephalopathy. Five patients died within the first 9 years of life and none achieved developmental, communicative or motor skills following birth. These clinical findings are consistent with a developmental brain disorder that begins in the prenatal brain, prevents neural connections from reaching the expected stages at birth, and follows a progressive course. DMXL2 is highly expressed in the brain and at synaptic terminals, regulates v-ATPase assembly and activity and participates in intracellular signalling pathways; however, its functional role is far from complete elucidation. Expression analysis in patient-derived skin fibroblasts demonstrated absence of the DMXL2 protein, revealing a loss of function phenotype. Patients' fibroblasts also exhibited an increased LysoTracker® signal associated with decreased endolysosomal markers and degradative processes. Defective endolysosomal homeostasis was accompanied by impaired autophagy, revealed by lower LC3II signal, accumulation of

polyubiquitinated proteins, and autophagy receptor p62, with morphological alterations of the autolysosomal structures on electron microscopy. Altered lysosomal homeostasis and defective autophagy were recapitulated in Dmxl2-silenced mouse hippocampal neurons, which exhibited impaired neurite elongation and synaptic loss. Impaired lysosomal function and autophagy caused by biallelic DMXL2 mutations affect neuronal development and synapse formation and result in Ohtahara syndrome with profound developmental impairment and reduced life expectancy.

Lugarà E, **De Fusco A**, Lignani G, Benfenati F, Humeau Y. Synapsin I Controls Synaptic Maturation of Long-Range Projections in the Lateral Amygdala in a Targeted Selective Fashion. Front Cell Neurosci. 2019 May 21;13:220. doi: 10.3389/fncel.2019.00220.

The amygdala, and more precisely its lateral nucleus, is thought to attribute emotional valence to external stimuli by generating long-term plasticity changes at long-range projections to principal cells. Aversive experience has also been shown to modify pre- and post-synaptic markers in the amygdala, suggesting their possible role in the structural organization of adult amygdala networks. Here, we focused on how the maturation of cortical and thalamic long-range projections occurs on principal neurons and interneurons in the lateral amygdala (LA). We performed dual electrophysiological recordings of identified cells in juvenile and adult GAD67-GFP mice after independent stimulation of cortical and thalamic afferent systems. The results demonstrate that synaptic strengthening occurs during development at synapses projecting to LA principal neurons, but not interneurons. As synaptic strengthening underlies fear conditioning which depends, in turn, on presence and increasing expression of synapsin I, we tested if synapsin I contributes to synaptic strengthening during development. Interestingly, the physiological synaptic strengthening of cortical and thalamic synapses projecting to LA principal neurons was virtually abolished in synapsin I knockout mice, but not differences were observed in the excitatory projections to interneurons. Immunohistochemistry analysis showed that the presence of synapsin I is restricted to excitatory contacts projecting to principal neurons in LA of adult mice. These results indicate that synapsin I is a key regulator of the maturation of synaptic connectivity in this brain region and that is expression is dependent on postsynaptic identity.

Articles published by Antonio De Fusco during the PhD course due to previous work.

Biagioni F, Gaglione A, Giorgi FS, Bucci D, Moyanova S, **De Fusco A**, Madonna M, Fornai F. Degeneration of cholinergic basal forebrain nuclei after focally evoked status epilepticus. Neurobiol Dis. 2019 Jan;121:76-94. doi: 10.1016/j.nbd.2018.09.019.

Status epilepticus (SE) of limbic onset might cause degenerative phenomena in different brain structures, and may be associated with chronic cognitive and EEG effects. In the present study SE was evoked focally by microinfusing picomolar doses of cyclothiazide+bicuculline into the anterior extent of the piriform cortex (APC) in rats, the so-called area tempestas, an approach which allows to evaluate selectively the effects of seizure spreading through the natural anatomical circuitries up to secondary generalization. In the brain of rats submitted to SE we analyzed neuronal density, occurrence of degenerative phenomena (by Fluoro-Jade B-FJB- staining) and expression of heat shock protein-70 (HSP-70) in the piriform cortex, the hippocampus and ventromedial thalamus. We further analyzed in detail, the loss of cholinergic neurons, and the presence of FJB- and HSP-70 positive neurons in basal forebrain cholinergic areas, i.e. the medial septal nucleus (MSN, Ch1), the diagonal band of Broca (DBB, Ch2 and Ch3) and the Nucleus basalis of Meynert (NBM, Ch4). In fact, these nuclei are strictly connected with limbic structures, and play a key pivotal role in different cognitive functions and vigilance. Although recent studies begun to investigate these nuclei in experimental epilepsy and in persons with epilepsy, conflicting results were obtained so far. We showed that after severe and long-lasting, focally induced limbic SE there is a significant cell loss within all of the abovementioned cholinergic nuclei ipsi- and contra-laterally to the infusion site. In parallel, these nuclei show also FJB and heat shock protein-70 expression. Those effects vary depending on the single nucleus assessed and on the severity of the SE seizure score. We also showed the occurrence of cell loss and degenerative phenomena in limbic cortex, hippocampus and limbic thalamic areas. These novel findings show direct evidence of SE-induced neuronal damage which is solely due to seizure activity ruling out potential confounding effects produced by systemic pro-convulsant

neurotoxins. A damage to basal forebrain cholinergic nuclei, which may underlie cognitive alterations, is documented for the first time in a model of SE triggered focally.

Moyanova S[#], **De Fusco A**[#], Santolini I, Celli R, Bucci D, Mastroiacovo F, Battaglia G, Nicoletti F, Tchekalarova J. Abnormal Hippocampal Melatoninergic System: A Potential Link between Absence Epilepsy and Depression-Like Behavior in WAG/Rij Rats? Int J Mol Sci. 2018 Jul 6;19(7). pii: E1973. doi: 10.3390/ijms19071973.

#: equal contribution

Absence epilepsy and depression are comorbid disorders, but the molecular link between the two disorders is unknown. Here, we examined the role of the melatoninergic system in the pathophysiology of spike and wave discharges (SWDs) and depression-like behaviour in the Wistar Albino Glaxo from Rijswijk (WAG/Rij) rat model of absence epilepsy. In WAG/Rij rats, SWD incidence was higher during the dark period of the light-dark cycle, in agreement with previous findings. However, neither pinealectomy nor melatonin administration had any effect on SWD incidence, suggesting that the melatoninergic system was not involved in the pathophysiology of absence-like seizures. Endogenous melatonin levels were lower in the hippocampus of WAG/Rij rats as compared to non-epileptic control rats, and this was associated with higher levels of melatonin receptors in the hippocampus, but not in the thalamus. In line with the reduced melatonin levels, cell density was lower in the hippocampus of WAG/Rij rats and was further reduced by pinealectomy. As expected, WAG/Rij rats showed an increased depression-like behaviour in the sucrose preference and forced swim tests, as compared to non-epileptic controls. Pinealectomy abolished the difference between the two strains of rats by enhancing depression-like behaviour in non-epileptic controls. Melatonin replacement displayed a significant antidepressant-like effect in both WAG/Rij and control rats. These findings suggest that a defect of hippocampal melatoninergic system may be one of the mechanisms underlying the depression-like phenotype in WAG/Rij rats and that activation of melatonin receptors might represent a valuable strategy in the treatment of depression associated with absence epilepsy.